*Advances in Colloid and Interface Science*, 28 (1988) 249–331
Elsevier Science Publishers B.V., Amsterdam — Printed in The Netherlands



# FRACTAL AGGREGATES

Paul Meakin
Central Research and Development Department, E. I. du Pont de Nemours and Company, Wilmington, DE 19898

CONTENTS

## I. ABSTRACT

In recent years it has been shown that the structures of a wide variety of colloidal aggregates can be described in terms of the concepts of fractal geometry. The purpose of this review is to discuss some of the evidence for fractal geometry in experimental systems and indicate how fractal geometry can be used to develop a better understanding of their aggregation kinetics and physical properties. At the present time much of our understanding of the structure and properties of fractal aggregates has come from computer simulations. Consequently, a major part of this paper is concerned with the role played by simple computer models in understanding the origins of fractal aggregates as well as their physical and chemical properties. The main emphasis is on models for colloidal aggregation but a brief description of a few other models for non-equilibrium growth and aggregation processes which have been of particular interest during the past few years has been included.

## II. INTRODUCTION

The aggregation of small particles to form larger structures is a process of considerable importance in many areas of science and technology. The resulting flocs or aggregates frequently have a complex random structure with a low average density. Such systems are often described by qualitative terms such as wispy, ramified or tenuous. Figure 1 shows a gold particle aggregate consisting of almost spherical gold particles with an average diameter of about 100Å [ref. 1]. The low density ramified structure of this aggregate is typical of the systems with which this review is concerned.

The lack of a quantitative description of random aggregates has inhibited the development of a systematic understanding of

their properties. Recently, it has been recognized that some aspects of the structure of a variety of aggregated systems can be described in terms of the concepts of fractal geometry [refs. 2-4]. Fractal geometry does not provide us with a complete description of the structure of flocculated colloids. However, it does provide a basis for developing a better understanding of many of the most important properties of at least some types of aggregates. The purpose of this review is to present some of the evidence for fractal geometry in colloidal aggregates and to discuss the implications of this fractal structure for physical (and chemical) properties and aggregation kinetics.

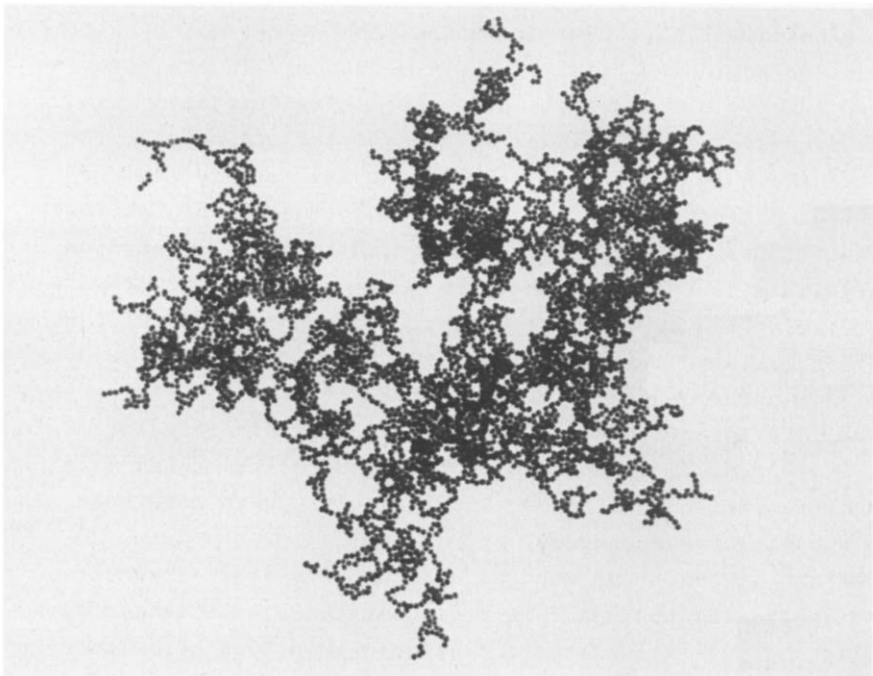

Fig. 1. A gold particle aggregate consisting of 4739 spherical gold particles with a diameter of about 100Å. This aggregate was formed from a stable aqueous dispersion of gold particles by adding pyridine to displace charges adsorbed on their surfaces. The figure shows a transmission electron micrograph which represents a projection of the three dimensional aggregate onto a plane. This figure was provided by D. A. Weitz and is reproduced with permission.

During recent years considerable interest has developed in fractal geometry and its applications to physics and chemistry. Several books have been published on the subject of fractal

geometry [refs. 2-8] and a number of books [refs. 8 and 9], conference proceedings [refs. 10-15] and reviews [refs. 16-26] concerned with fractal aggregates and other random systems have also appeared.

The current high level of interest in fractal aggregates has resulted from the development of the concepts of fractal geometry (primarily by B. B. Mandelbrot who invented the term fractal and has more recently popularized fractal geometry in a beautifully illustrated series of books [refs. 2-4]), a generally enhanced interest in random systems (because of their practical and scientific importance) and the development of the diffusion limited aggregation model (DLA) by Witten and Sander [ref. 27]. In the DLA model particles are added, one at a time, to a growing cluster or aggregate of particles via random walk trajectories. Figure 2 shows a cluster of 10,000 particles generated using a three dimensional off-lattice version of the DLA model. The cluster shown in Figure 2 does have the low density tenuous structure characteristic of colloidal aggregates such as that shown in Figure 1. However, even the most casual comparison of Figures 1 and 2 indicates that the DLA model does not provide a good description of the type of colloidal aggregates which are the main concern of this review. The DLA model does provide a basis for understanding a broad variety of other phenomena in colloid and interface science. It also provides stimulation for the development of other models which led to structures more closely resembling that shown in Figure 1. These models are the main subject of this review.

At the present time much of what we know about fractal colloidal aggregates has come from computer simulations. These simulations have stimulated and have in turn been stimulated by the careful investigation of a variety of real systems and theoretical work. Since aggregating systems are often complex and difficult to control, the results of computer simulations are often of more value than experiments for the purpose of evaluating theoretical ideas. However, the ultimate objective of this work is to develop a comprehensive theoretical understanding of aggregation processes which can be used to describe and guide experimental work.

At the present time our understanding of even the most simple non-equilibrium growth and aggregation models is far from

complete. Although some models are quite well understood, there are no generally successful theoretical approaches which can be used to calculate the geometric scaling properties of aggregates from the algorithm used to generate them. Consequently, this review is concerned primarily with computer simulations and experimental studies. However, if the geometric scaling properties are known, it is generally possible to obtain an adequate theoretical understanding of the aggregation kinetics and a wide variety of physical properties. Some recent advances in this direction are also discussed.

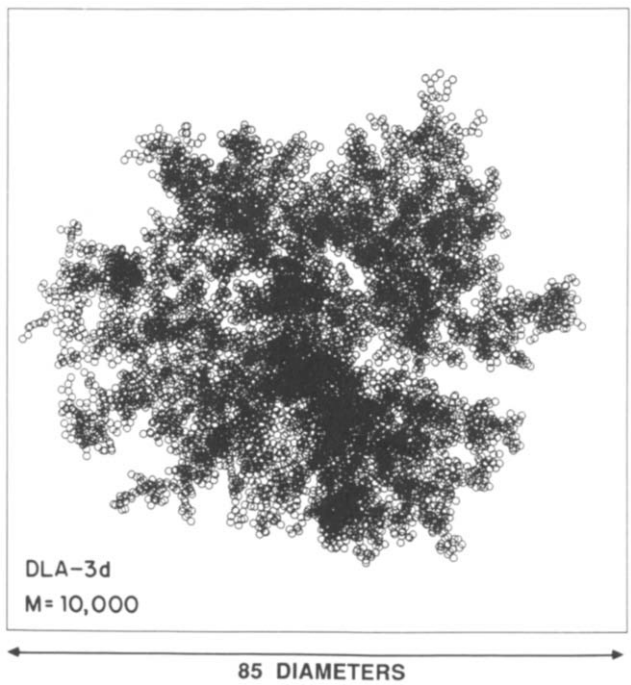


Fig. 2. A cluster of 10,000 particles generated by a three dimensional off-lattice model for diffusion-limited aggregation (DLA). In this model particles are added, one at a time, to the growing cluster or aggregate via random walk trajectories originating far from the cluster.

## III. FRACTAL GEOMETRY

The structures of a very wide variety of familiar objects (mountains, clouds, coastlines, rivers, the vascular system and other biological structures, etc.) and systems of scientific interest (macromolecules, gels, turbulence, "strange" attractors,

rough surfaces, etc.) cannot readily be described in terms of the concepts of Euclidean geometry. During the past 2-3 decades a new geometry which provides a basis for describing and understanding many of these structures and processes has been developed by Mandelbrot [refs. 2-4]. In recent years this "fractal" geometry has been found to be relevant to an extremely broad range of systems and phenomena of scientific interest. The scope of fractal geometry and the extent to which it can be applied to real systems is still being explored. In this section those aspects of fractal geometry which have been found to be the most relevant to colloidal aggregation and colloidal aggregates are outlined.

A. General Principles

Fractal geometry is concerned with geometric scaling relationships and the symmetries associated with them. Most of the familiar objects mentioned in the previous section are invariant to a change of length scale (at least to a good approximation for some limited range of length scales). A consequence of this scale invariance or self-similarity is that these objects look the same under different magnifications. The implications of this symmetry are similar to the implications of the more familiar symmetries (rotation, reflection, inversion and translation) associated with Euclidean systems. Using group theory we can understand many of the important properties of Euclidean objects without a detailed knowledge of their physics. Understanding at this level plays a vital role in quantum mechanics, spectroscopy, crystallography, reaction mechanisms and many other areas. In a similar way fractal geometry can be used to understand many aspects of the physical behavior of fractal structures. Knowledge of the fractal dimensionality alone allows us to make important statements about the way in which the fractal will interact with particles waves and fields and the way in which properties like the hydrodynamic radius depend on the mass of the fractal. Other fractal scaling relationships (such as the dependence of the minimum path length on the fractal between two points on their separation measured in the embedding space or lattice and the fracton dimensionality (section IIID)) provide a basis for understanding properties such as conductivity, vibrational density of states and mechanical properties. The laws of physics describing the behavior of

ordinary Euclidean systems may be regarded as a special case for the corresponding laws for fractal systems. Very often these laws are quite different for fractal structures than for Euclidean systems. Much of the recent work on the physics of fractals has been directed towards an elucidation of these fundamental laws.

B. Self Similar Fractals

The most simple fractals are invariant under isotropic dilation or contraction. Figure 3 shows four stages in the construction of a self-similar fractal [refs. 28 and 29]. The example which has been selected can be considered to represent a very simple, highly organized aggregation process. In the first stage (Figure 3a), five discs are joined together to form a cluster. Four of the discs contact (but do not overlap) the fifth disc and their centers lie at the corners of a square. In the second stage (Figure 3b) five clusters each containing five discs are joined in a similar fashion to form a cluster of 25 discs. In the third stage (Figure 3c) five clusters each containing 25 discs are joined to form a cluster of 125 discs. At each stage in the construction the maximum diameter of the cluster of discs increases by a factor of 3 and the number of discs increases by a factor of 5. Figure 3 shows the first four generations in a process which can, in principle, be continued for an indefinitely large number of generations (N) leading to an "aggregate" containing $5^N$ discs with a diameter of $3^N$ disc diameters ($d_o$). The hierarchical structure formed in this fashion can also be extended to arbitrarily small length scales by replacing each of the discs by five smaller discs each having a diameter of $d_o/3$, etc. We can imagine extending these processes to infinitely large and infinitesimally small length scales leading to the generation of a self-similar fractal. In this particular case, five replicas of the fractal are required to cover itself after dilation by a factor of 3 and the fractal dimensionality (D) is given by

$$D = \log(5)/\log(3) \simeq 1.465 \quad . \tag{1}$$

This "definition" of the fractal dimensionality is in accord with our intuitive understanding of dimensionality in Euclidean objects. For example, if a d dimensional hypercube is dilated by a factor of $\ell$ in all directions, it can be covered by $\ell^d$ replicas of the original (undilated) hypercube and the (Euclidean)

dimensionality (d) is given by

$$d = \log(\ell^d)/\log(\ell) \quad . \tag{2}$$

In general, if a self-similar fractal can be covered by N replicas of itself after an isotropic dilation by a factor of $\ell$, the fractal dimensionality is given by

$$D = \log(N)/\log(\ell) \quad . \tag{3}$$

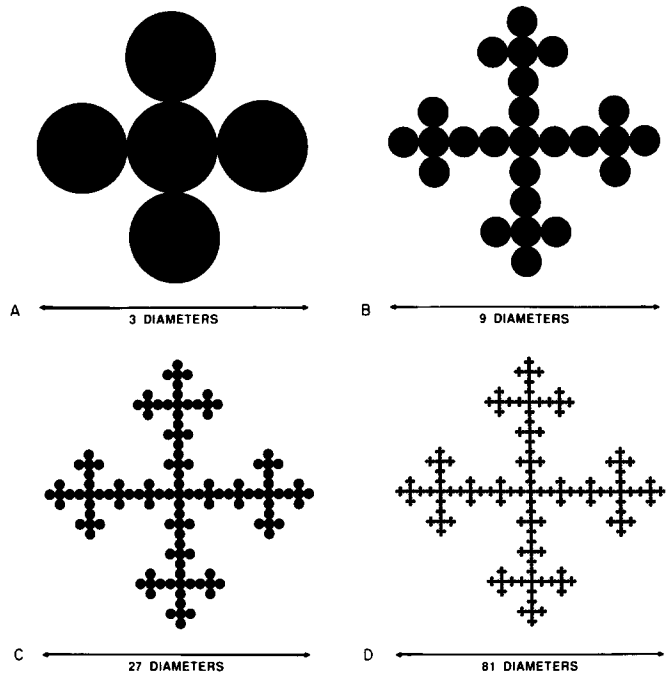


Fig. 3. Four stages in the construction of a simple deterministic fractal model for particle aggregates. In Figure 3a five particles have been joined to form a "cross". In Figure 3b five of these crosses have been joined to form a larger cross containing 25 particles. Figures 3c and 3d show the third and fourth stages of the hierarchical generation process which takes place in a two-dimensional embedding space (plane). Each time the mass is increased by a factor of 5 the overall size (length) of the aggregate increases by a factor of 3. The fractal dimensionality is given by $D = \log(5)/\log(3) \simeq 1.465$.

The ideas outlined above cannot be applied directly to most structures found in nature. For example, colloidal aggregates have a random structure much different from the regular structure shown in Figure 3 and there is no exact self-similarity (the structure cannot be mapped onto itself after dilation or contraction). Instead, we (may) have an average or statistical

self similarity. This means that the correlation functions which describe the structure of fractal aggregates have a scale invariant (power law) form. For example, the two point density-density correlation function C(r) for points separated by a distance r has the form

$$\langle C(r) \rangle \sim r^{-\alpha} \quad , \tag{4}$$

where the exponent $\alpha$ is given by $\alpha = D_{\alpha} - d$.

It is also important to recognize that for statistically self-similar fractals found in nature, geometric scaling relationships such as Equation (4) are not valid for all length scales (r). In the case of a colloidal aggregate consisting of particles with a radius $r_o$ and having an overall radius of $R_o$ Equation (4) is correct only for length scales ($\ell$) in the range $r_o \ll \ell \lesssim R_o$. For length scales smaller than $r_o$ the structure is uniform (D=d). In practice the self similarity (scale invariance) may end at length scales considerably smaller than $R_o$ as a result of physical processes such as collapse under gravity, the effects of thermal fluctuations or shear flow [refs. 30 and 31].

For colloidal aggregates and other random fractals in real space it is convenient to think of the fractal dimensionality in terms of the scaling relationship between mass (M) and length ($\ell$).

$$M \sim \ell^{D} \quad . \tag{5}$$

Relationships of this type are frequently employed to measure the fractal dimensionality. For example, if the radius of gyration ($R_g$) is measured as a function of the aggregate mass (M) and

$$\langle R_g \rangle \sim M^{\beta} \quad , \tag{6}$$

then the power law relationship between $R_g$ and M can be characterized by the fractal dimensionality $D_\beta$ given by $D_\beta = 1/\beta$ [ref. 32]. Similarly, if we find that the mass M contained within a distance $\ell$ measured from a position which is occupied by one of the particles is given by

$$\langle M \rangle \sim \ell^{\gamma} \tag{7}$$

then the corresponding fractal dimensionality is given by $D_\gamma = \gamma$. A third approach to measure the fractal dimensionality is to use the two point density-density correlation function C(r) which may be measured in a scattering experiment or calculated from the particle coordinates generated in a simulation or obtained from a digitized image. If the correlation function has the form given

in Equation (4), an effective fractal dimensionality ($D_\alpha$) is given by $D_\alpha = d-\alpha$. For self similar fractals $D_\alpha = D_\beta = D_\gamma = D$ where D is the "all purpose" fractal dimensionality [ref. 33]. Most measurements of the fractal geometry of real and simulated aggregates are based on Equations (5), (6) and (7).

For self-similar fractal aggregates many of the geometric scaling relationships are known if D has been measured. This provides us with the (asymptotic) form for the mass dependence of many important physical properties. For example, the hydrodynamic radius $R_h$ is given by

$$R_h \sim M^{1/D} \quad . \tag{8}$$

The area ($\sigma$) of a projection of the cluster onto a plane is given by

$$\sigma \sim M \quad \text{for } D \leqslant 2 \tag{9a}$$

$$\sigma \sim M^{2/D} \quad \text{for } D \geqslant 2 \tag{9b}$$

and the scattering of light, x-rays and neutrons is determined by the two point density-density correlation function (see equation (4)). It is for this reason that knowledge of the fractal dimensionality is important in understanding the properties of colloidal aggregates.

C. Self-Affine Fractals

Self-similar fractals are invariant under isotropic changes of length scale. In general, the transformations which rescale the structure of fractal objects are not isotropic and more than one fractal dimension or scaling exponent is required. A simple example is provided by the Brownian "process" B(t) which describes the distance travelled by a particle undergoing Brownian motion in a time t. The statistical properties of B(t) and $b^{-1/2}$ B(bt) are indistinguishable. This means that B(t) is invariant to a change in the horizontal (time) scale by a factor of b and a simultaneous change in the vertical scale by a factor of $b^{1/2}$. Since t and B(t) rescale differently the Brownian process is not self similar. The measurement and characterization of self-affine fractals requires more care than the determination of the all purpose fractal dimensionality (D) for self similar fractals. For example, the fractal properties of B(t) can be explored by covering the curve B(t) by boxes of size r. If N(r) is the number of boxes of size r required to cover the fractal, a "global" dimensionality ($D_G$) can be defined as

$N(r) \sim r^{-D_G}$, in the limit $(r \to \infty)$ . (10)

It is evident from the scaling properties of B(t) that $D_G = 1$. Similarly, a local dimensionality $D_L$ can be measured from

$N(r) \sim r^{-D_L}$ $(r \to 0)$ (11)

and $D_L$ has a value of 1.5.

Self-affine fractal geometry has been found to be an appropriate way of describing a wide variety of rough surfaces including mountains [ref. 2], ballistic deposits [refs. 34 and 35] and fracture surfaces [refs. 35,36]. Aggregates may be formed from rough particles whose surfaces can be described in terms of self affine fractal geometry. In addition, the surfaces of compact aggregates formed by ballistic aggregation [ref. 37] or Eden growth [ref. 38] have a self-affine fractal geometry.

The structure of most of the aggregates with which this review is concerned can be described well in terms of self similar fractal geometry. Consequently, only a brief discussion of self-affine fractal geometry is given here. More complete discussions can be found elsewhere [refs. 2-4, 33, 39-41].

D. Properties of Fractal Aggregates

Many of the properties of fractal aggregates are quite different from those of compact Euclidean objects. In those cases where D<d the "average" density ($\rho$) becomes smaller as the aggregate becomes larger according to the power law relationships

$\rho \sim \ell^{(D-d)}$ (12a)

or

$\rho \sim M^{(D-d)/D}$ . (12b)

This relationship has a number of important consequences. Because of their low density fractal aggregates are often mechanically weak structures which can be easily distorted and collapse as a result of gravitational fields, thermal fluctuations, etc. These effects limit the range of length scales over which fractal scaling can be maintained in real systems [ref. 30]. The low density and low mechanical strength of fractal aggregates is exploited in the use of fumed silica and other colloidal additives to control the rheology of paints, other coating systems, food products, etc. At low shear rates the particles and/or clusters aggregate to form a tenuous network which can be easily disrupted at higher shear rates. This behavior leads to a system which has a low viscosity at high shear rates and a high viscosity at low shear rates. In

addition, only small quantities (often <1% by volume) are needed to achieve the required level of rheology control for these applications.

Another important property associated with fractals is the scaling relationship between the minimum path length ($\ell$) measured on the fractal and the Pythagorean distance r separating them in the embedding space or lattice. These two quantities are related by the power law [refs. 42 and 43].

$$\ell \sim r^{D_{min}} \tag{13}$$

where the exponent $D_{min}$ has a value which is greater than or equal to 1 (in most cases $D_{min} > 1$). This has important implications for properties such as thermal and electronic conductivity, mechanical properties and diffusion on the fractal.

For all Euclidean spaces or lattices the root mean square distance $\langle r^2 \rangle^{1/2}$ moved by a random walker after t steps (or after a time t) is given by:

$$\langle r^2 \rangle^{1/2} \sim t^{1/2} \quad . \tag{14}$$

This relationship between the rms displacement and time can be interpreted in terms of a fractal dimensionality $D_w$ for the random walk by rewriting Equation (14) in the form

$$\langle r^2 \rangle^{1/2} \sim t^{1/D_w} \quad . \tag{15}$$

Here $\langle r^2 \rangle^{1/2}$ is a characteristic distance associated with the walk and t (the number of steps) is analogous to the mass in Equation (5). For all Euclidean systems $D_w$ has a value of 2. For fractals $D_w$ is greater than 2 [ref. 44]. $D_w$ is greater than 2 because, in general, the fractal dimensionality $D_{min}$ defined in Equation (11) is greater than 1 and because of the many "dead ends" found in random fractals which act like temporary traps for diffusion on the "backbone" of the fractal. The relatively high value of $D_w$ for diffusion on fractal substrates has important implications for processes such as diffusion-limited reactions, exciton transport and annihilation, energy transfer, trapping processes, electronic conductivity, etc. Even a brief discussion of these implications is beyond the scope of this review. Additional information can be found in other reviews [ref. 45].

It is often convenient to rewrite Equation (13) as

$$\langle r^2 \rangle^{1/2} \sim t^{D_s/2D} \quad . \tag{16}$$

Here $D_s$ is the spectral of fracton dimensionality ($D_s = 2D/D_w$) introduced by Alexander and Orbach [ref. 46]. The dimensionality $D_s$ can be measured directly in a random walk simulation since the

probability of return to the origin $F_o(n)$ after n steps is given by [refs. 46,47]

$$F_o(n) \sim n^{-D_s/2} \quad , \tag{17}$$

and the mean number of distinct sites s visited by the random walk is given by

$$s \sim n^{D_s/2} \tag{18}$$

The random walk process can be described in terms of a master equation for the probability $P_i(t)$ that the ith position will be occupied at time t

$$d/dt(P_i) = \sum_j (W_{ji}P_j(t) - W_{ij}P_i(t)) \quad . \tag{19}$$

A similar equation describes the propagation of vibrational excitation (within the harmonic approximation [ref. 48]

$$d^2(\delta_i)/d_t^2 = \sum_j (K_{ji}\delta_j - K_{ij}\delta_i) \quad , \tag{20}$$

where the $\delta_i$ are the displacements associated with the vibrational excitation [ref. 48]. The matrices $\underset{\approx}{W}$ and $\underset{\approx}{K}$ have the same structure. Consequently, an intimate relationship exists between diffusion on a fractal network and the propagation of phonons on the same network [ref. 49].

For a vibrating Euclidean network the density of state at low frequencies $\omega$ is given by

$$N(\omega) \sim \omega^{d-1} \quad . \tag{21}$$

Alexander and Orbach [ref. 46] have shown that for a fractal the equation must be replaced by

$$N(\omega) \sim \omega^{D_s-1} \quad , \tag{22}$$

where $D_s$ is the fracton or spectral dimensionality introduced in Equation (14). The vibrational density of states is important for processes such as thermal conductivity and properties such as the specific heat. The density of state $N(\omega)$ and hence $D_s$ can be measured using Brillouin scattering, neutron scattering, ultrasound attenuation, etc., as well as low temperature specific heat and thermal conductivity measurements. Additional information concerning diffusion and vibrational excitations on fractals can be found in recent reviews [refs. 23, 50 and 51].

Fractal geometry has important implications for the scattering of light and other radiation by aggregates. The scattering of light by aggregates is of interest for a number of reasons including its relevance to air and water pollution,

paints and pigments, smoke screens, the nuclear winter effect and many others. The scattering of radiation by fractal aggregates is also of considerable scientific interest since it provides one of the most important methods for characterizing the structure of fractal aggregates. For example, in many scattering experiments the scattered intensity S(k) for a wave vector of k ($k = 4\pi\sin(\theta/2)/\lambda$ where $\lambda$ is the wavelength and $\theta$ is the scattering angle) is determined by the Fourier transform of the two point density-density correlation function C(r) and S(k) has the power law form

$$S(k) \sim k^{-D} \tag{23}$$

Consequently, D can be determined from the dependence of S(k) on k. In practice S(k) exhibits the power law form given in Equation (21) over only a limited range of wave vectors corresponding to the range of length scales over which the aggregate exhibits fractal scaling. The interpretation of small angle scattering experiments can be quite difficult and care must be taken to include appropriate corrections for finite size effects and short range correlations [refs. 52 and 53].

Berry and Percival [ref. 54] have examined theoretically the scattering of light by random fractal aggregates consisting of refracting and absorbing spherical particles under the conditions $ka \ll 1$ (where a is the particle radius). The overall cluster size, given by $R \simeq a N^{1/D}$ where N is the number of particles, may be larger than the wavelength. They find that for both scalar and vector waves the scattering cross-section for a cluster with $D<2$ is asymptotically proportional to the number of particles but that the scattering per particle (for $N \to \infty$) is larger than that for a single particle by a factor or order $(ka)^{-(3-D)}$. For $D>2$ the scattering per particle is proportional to $N^{1-2/D}$. In this analysis the effects of multiple scattering were neglected. These results indicate that scattering by fractal aggregates is very much different from scattering by compact aggregates (D=3) particularly if $D<2$. Interest has also developed in the possibility of using second order or collision induced light scattering to obtain more detailed information concerning the structure of fractal aggregates [refs. 55 and 56] and in the effects of rotational diffusion on light scattering by anisotropic aggregates [refs. 31 and 57].

Many other properties associated with fractal structures are quite different from those found in ordinary Euclidean objects.

These include phase transitions and critical phenomena, wetting, adsorption of small molecules, third sound, capillary condensation and many others. Unfortunately, the limited length of this review precludes even a brief survey of these very interesting phenomena. One implication of fractal geometry which will be discussed in some detail is its relevance to the kinetics of colloid aggregation. Fractal geometry is important in colloid aggregation primarily because of its effects on collision cross sections and on the rates at which clusters move (cluster diffusion coefficients).

One of the most important characteristics of random fractals is the large spatial and sample-to-sample fluctuations in their properties. For this reason most of the equations written above do not apply to individual realizations. They are relationships between quantities which have been averaged over a large ensemble. However, the ensemble average symbols <--> have been omitted from these equations to obtain a more compact notation. The fluctuation associated with fractal structures are not merely an inconvenience which makes it more difficult to determine the power law relationships which characterize these systems, they are in fact important quantities in their own right which provide a more complete description of the aggregates and have significant implications for their properties [refs. 2 and 58].

## IV. EARLY MODELS AND EXPERIMENTS

The concepts of fractal geometry have only become widely disseminated in recent years following the publication of Mandelbrot's books [refs. 2-4]. However, the geometry of colloidal aggregates has been of interest for many years and some of the early work on real and simulated colloidal aggregates can now be reinterpreted in terms of fractal geometry. Simple computer models for colloidal aggregation have been studied for more than a quarter of a century. Now that it is generally recognized that many naturally occurring systems exhibit fractal scaling over a significant range of length scales, it is natural to ask why fractal structures are so common. A partial answer to this question is provided by the observation that many simple models for growth and aggregation lead to structures with a well defined fractal geometry.

### A. Ballistic Growth and Deposition

In the ballistic aggregation model [ref. 59], particles are added, one at a time, to a growing cluster or aggregate of

particles via randomly selected ballistic (linear) trajectories. The particles are added irreversibly at the position in which they first contact the growing cluster. Figure 4 shows a cluster of 10,000 particles grown using a three dimensional off-lattice version of this model. Vold [ref. 59] carried out simulations using this model which indicated that the number of particles $N(\ell)$ within a distance $\ell$ measured from the first particle ("seed" particle) in the cluster was given by

$$N(\ell) \sim \ell^{2.3} \quad . \tag{24}$$

This result could be interpreted in terms of a fractal dimension of 2.3 (compare with Equation (7)). However, Sutherland [ref. 60] pointed out that the random walk trajectories used by Vold were not properly selected from a random distribution and concluded on the basis of simulations carried out using up to 2000 particles that D=d for d=2 and 3. Despite the simplicity of this model, it is not easy to obtain accurate values for the asymptotic fractal dimensionality because of surprisingly large corrections to scaling. It is only quite recently, on the basis of large scale simulations [refs. 61, 62] and theoretical arguments [refs. 63, 64] that a concensus that D = d for this model has developed.

Vold also developed a variety of ballistic deposition models to simulate sedimentation processes. A density of 0.128 was found for deposition of spherical particles via vertical paths onto a horizontal surface [ref. 37]. Densities of 0.128 to 0.0146 were found for the deposition of anisometric particles with aspect ratios varying from 1-18 [ref. 65]. Much larger scale simulations give a density of about 0.146 for the deposition of spherical particles [ref. 66].

Although the internal structure of ballistic aggregates and deposits is uniform on all but short length scales, the surfaces of these structures have a self-affine fractal geometry which is now the subject of considerable interest [refs. 34, 67-69]. Most of the early simulation work was carried out using off-lattice models. Lattice models are considerably more simple but less realistic. Because of their simplicity, they can be used to generate very large deposits ($\simeq 10^{10}$ sites) which are often needed to explore asymptotic scaling relationships. These relationships are generally assumed to be universal (independent of model details such as lattice structure). However, there is at present

no good theoretical reason for assuming that the concept of universality applies to non-equilibrium growth models in general. In fact, in some cases the best computer simulation results indicate that the scaling exponents characterizing fractal geometry may have at best a very narrow range of universality. However, in the case of ballistic deposition the universality concept does seem to be valid and it also seems that the Eden growth model [ref. 38] and ballistic growth model belong to the same universality class (in the sense that all of the exponents associated with their geometry have the same values (see refs. 67-70)).

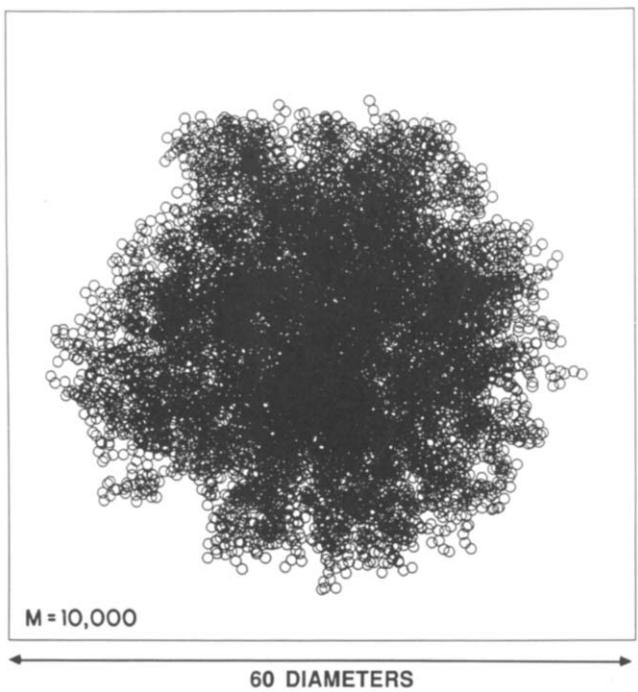


Fig. 4. A cluster of 10,000 identical spherical particles generated by a three dimensional off-lattice model for ballistic particle-cluster aggregation.

B. Ballistic Cluster-Cluster Aggregation

A very successful ballistic cluster-cluster aggregation model was developed by Sutherland [refs. 71-73]. In this model pairs of clusters are selected from a list of clusters, brought together via randomly selected ballistic trajectories (after rotation to random orientations) and returned to the list which

now contains one less member. The simulation starts with $N_o$ single particles and ends when two clusters are brought together to form a single cluster containing all $N_o$ particles. Sutherland investigated several versions of this model which differ in the way in which clusters are selected. One version of this model corresponds to Vold's ballistic aggregation model discussed above. In another version of the model the pairs of clusters are selected with probabilities given by the Smoluchowski equation [refs. 74 and 75] for ballistic aggregation. In the third version (called the maximum chain model by Sutherland but now known as the hierarchical model) the system starts with $N_o = 2^N$ particles which are combined to form $2^{N-1}$ binary clusters. These binary clusters are then added pairwise via linear trajectories to form $2^{N-2}$ four particle clusters, etc. In this model the pairs of clusters combined at the kth generation each have $2^{k-1}$ particles whereas in the previous model the cluster size distribution becomes polydisperse at intermediate stages. Both of these models are called cluster-cluster aggregation models to distinguish them from the particle-cluster ballistic aggregation model of Vold [ref. 37].

The dependence of both the maximum radius and the radius of gyration on the cluster mass (number of particles) was measured for both cluster-cluster ballistic aggregation models. In both cases an exponent with a value of 0.54 (corresponding to an effective fractal dimensionality of about 1.85) was obtained from simulations carried out using up to 256 particles. More recently, much larger scale simulations indicate that $D \simeq 1.90$ for the hierarchical model and $D \simeq 1.95$ for the polydisperse model [refs. 76 and 77]. The differnce between these fractal dimensionalities is several times their combined statistical uncertainty, and it appears that this model is not universal. It seems intuitively reasonable that the polydisperse model should give a higher fractal dimensionality since small clusters can penetrate further into large clusters than clusters of comparable size can interpenetrate.

C. Experimental Evidence for Fractal Geometry

The concepts of fractal geometry have become widely disseminated only in recent years. However, mass-length scaling relationships which would now be recognized as indicating a fractal geometry were found earlier in a variety of systems.

Almost 25 years ago Beeckmans [ref. 78] proposed a

hierarchical model for a variety of particle aggregates. For aggregates described by Beeckmans' model the mean aggregate density ($\rho$) is given by

$$\rho \sim M^{-\bar{\lambda}} \quad , \tag{25}$$

where M is the aggregate mass. The power law relationship between $\rho$ and M given in Equation (25) is characteristic of a fractal with a dimensionality given by $D_{\bar{\lambda}} = d/(1+\bar{\lambda})$. According to Beeckmans' model, the parameter $\bar{\lambda}$ can lie in the range $0 \leq \bar{\lambda} \leq 0.64$ corresponding to fractal dimensionalities (for d = 3) in the range $1.83 \leq D \leq 3.0$. Using data available in the literature (1922-1961) Beeckmans obtained values for $\bar{\lambda}$ of 0.74 for MgO, 0.23 for tungsten, 0.19 for selenium, 0.78 for platinum, 1.7 for gold and 0.33 for $HgCl_2$. The uncertainties in these values for $\bar{\lambda}$ were quite large and the data available in 1964 were not adequate to support the proposed power law relationship between mass and density.

In an extensive series of publications spanning more than a decade, Medalia described a variety of ways of describing the structures of particle aggregates (particularly carbon particle aggregates [refs. 79-81]). Using a ballistic particle-cluster aggregation model, Medalia [ref. 82] found that the projected area ($\sigma$) of a cluster was related to the number of particles (s) or mass (M) by

$$\sigma \sim M^{0.87} \quad , \tag{26}$$

and this result was used to compute the number of particles in an aggregate from its projected area [ref. 83]. The power law relationship between $\sigma$ and M given in Equation (26) could be interpreted in terms of a fractal dimensionality of 2/0.87 or about 2.3. However, the clusters used by Medalia were much too small to be near to the asymptotic scaling regime (for either the simulations or experiments). It is now generally accepted that the fractal dimensionality for a ballistic particle-cluster aggregation is equal to the Euclidean dimensionality (D=d) [refs. 61-64]. For D=d=3 we would expect to find that

$$\sigma \sim M^{0.667} \tag{27}$$

for $M \to \infty$. However, the effective exponent would be larger than 2/3 for small clusters. It also seems most unlikely that the carbon particle aggregates studied by Medalia were formed by a ballistic particle-cluster aggregation process. A ballistic cluster-cluster aggregation process seems much more probable (see section IVB).

## V. NON-EQUILIBRIUM GROWTH MODELS

Much of our present (still rather primitive) understanding of non-equilibrium processes has been gained by studying simple models using computer simulations and analytical methods. A large number of these models has now been developed to represent a wide variety of physical, chemical and biological processes. Even a superficial discussion of all of these models could not be contained in a review of reasonable length. In this section a few of these models are described. These models have been selected because of the current high level of interest in them, their fundamental importance and their relevance to colloid aggregation. A more comprehensive review of growth models has been prepared by Herrmann [ref. 16].

### A. The Eden Model

The Eden model [ref. 38,84] was developed to simulate the growth of cell colonies. At the start of the simulation, a single site on a lattice is occupied and its unoccupied nearest neighbors (perimeter sites are identified). One of these perimeter sites is then selected randomly and filled to represent the growth process. After each site has been filled, the new unoccupied perimeter sites are identified. In the original Eden model the perimeter sites were randomly selected with probabilities proportional to their number of occupied nearest neighbors. Today most simulations are carried out using a simplified version of this model in which the unoccupied perimeter sites are selected randomly with equal probabilities irrespective of their environment. A third version of these models [refs. 85 and 86] has recently been introduced in which occupied surface sites (sites with one or more unoccupied nearest neighbors) are selected at random and one of their unoccupied nearest neighbors is randomly selected and filled. This model seems to reduce the surprisingly large corrections to the asymptotic scaling properties associated with this model. The structures formed by the Eden models are completely dense (small holes are formed near to the outer surface but they rapidly become filled). Figure 5 shows a typical cluster of 10,000 occupied sites generated by the Eden model.

Quite recently two aspects of the structures generated by Eden models have attracted considerable attention. These are the presence of a small anisotropy in the surface growth velocity on

the square lattice [refs. 69, 87, 88] which results in a small distortion from the almost circular shape evident in Figure 5 and the self-affine fractal geometry of their surfaces. The self-affine fractal geometry of the cluster surfaces can be most conveniently studied by carrying out simulations on strips of width L lattice units using periodic boundary conditions. One of the manifestations of this self affine fractal geometry is the dependence of the surface thickness (variance in the surface height) on the strip width L and the height (h) of the growth process. Computer simulations carried out using the Eden model indicate that the surface thickness ($\xi$) can be described in terms of the scaling form [34]

$$\xi \sim L^{\alpha'} f(h/L^{\alpha'/\beta'}) \quad , \tag{28}$$

where f(x) is a scaling function. For large values of x ($h \gg L^{\alpha'/\beta'}$) f(x) has a constant value and $\xi \sim L^{\alpha'}$. For small values of x, f(x) grows algebraically with increasing x and the surface

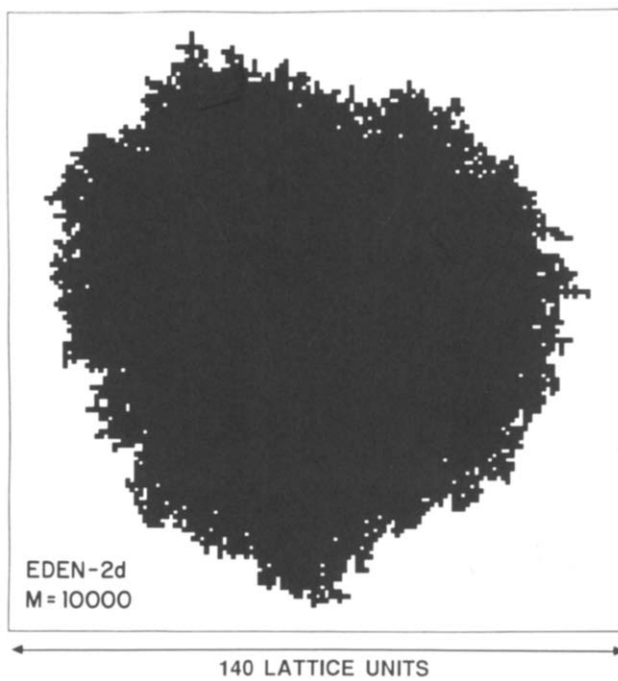


Fig. 5. A 10,000 site cluster generated by a two-dimensional Eden model. In the version used to generate this figure all of the unoccupied perimeter sites have equal growth probabilities.

thickness depends only on h. These conditions require that $\xi \sim h^{\beta'}$. In two dimensions computer simulations [refs. 69, 85-93] and theory [ref. 67] indicate that $\alpha' = 1/2$ and $\beta' = 1/3$. In three dimensional systems the uncertainties are much larger but it seems that $\alpha' \simeq 1/3$ and $\beta' \simeq 1/4$ [refs. 68, 94]. There are strong indications that the Eden model and the ballistic growth and deposition models belong to the same universality class. This means that all of the geometric scaling properties expressed by the exponents D, $\alpha'$ and $\beta'$ (and other exponents [ref. 70]) have the same values for both models.

B. Diffusion Limited Aggregation

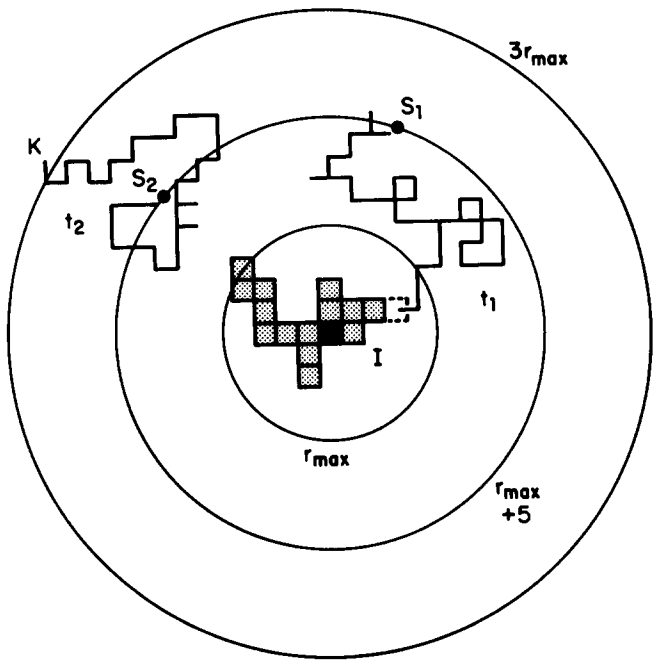


Fig. 6. An early stage in a square lattice model simulation of diffusion-limited aggregation. The original seed or growth site is shown in black and the other sites which are occupied at this stage are shaded. Two typical trajectories starting at random positions on the launching circle are shown. Trajectory $t_1$ reaches an unoccupied surface site (growth site), which is indicated by dashed edges, and this site is occupied. Trajectory $t_2$ reaches the termination circle which in this case has a radius of $3R_{max}$ where $R_{max}$ is the maximum radius of the cluster. This trajectory will be terminated and a trajectory started at a random position on the launching circle.

In the diffusion limited aggregation model of Witten and Sander [ref. 27] particles are added, one at a time, to a growing cluster or aggregate of particles via random walk trajectories. Figure 6 illustrates a two dimensional version of this model carried out on a square lattice. At the stage of growth illustrated in Figure 6 a small cluster has already formed. The particles are imagined to have come from infinity but are actually launched from a random position on a circle which just encloses the cluster (in this case this launching circle has a radius of $r_{max}$ + 5 lattice units, where $r_{max}$ is the maximum radius of the cluster measured from the original "seed" or growth site). Two typical random walk trajectories are shown in Figure 6. Trajectory $t_1$ eventually brings the random walker into an unoccupied perimeter site. At this stage this perimeter site is filled (growth occurs) and a new random walker is launched from the launching circle (whose radius increases as the cluster grows). Trajectory $t_2$ eventually moves the particle a long way from the cluster and this trajectory is terminated when it reaches the killing circle which has a radius of 3 $r_{max}$ in this simulation (this is satisfactory for small scale simulations but a more typical value for the radius of the killing circle in more recent large scale simulations is 100 $r_{max}$). The procedures described above and illustrated in Figure 6 are repeated many times until a large cluster has grown. Figure 7 shows a cluster of 50,000 sites grown using a similar algorithm on a six coordinate "honeycomb" lattice. From a large number of simulations similar to that illustrated in Figure 7, an effective fractal dimensionality ($D_\beta$) of 1.71 is obtained from the dependence of the radius of gyration on cluster mass (Equation (6)). From similar (off lattice) three dimensional simulations, a fractal dimensionality of 2.52 is obtained [ref. 95]. Many of the aspects of this model are of considerable current interest including the effects of lattice anisotropy, description of the growth probability distribution in terms of a fractal measure, the growth kinetics and the effects of finite particle concentrations. However, this model does not lead to the formation of structures which resemble those formed in most two dimensional or three dimensional aggregation processes. Information concerning recent work on this model can be found in a number of books and reviews [refs. 7-25, 96, 97].

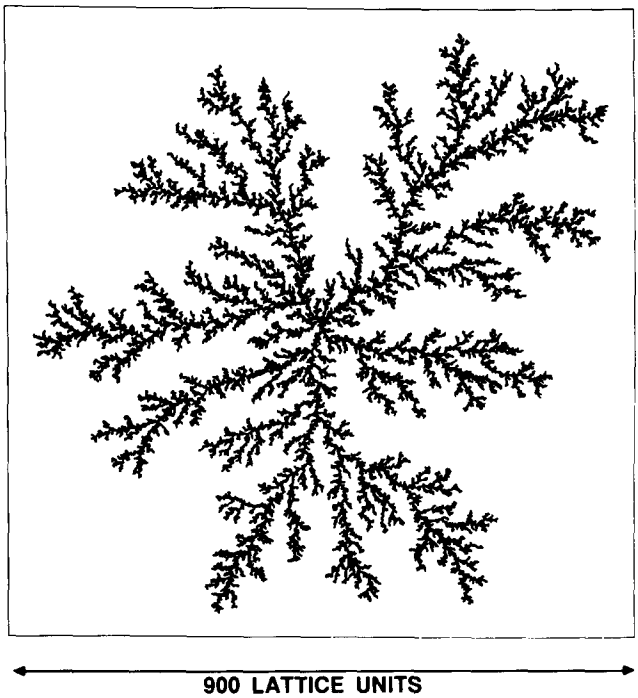


Fig. 7. A 50,000 site cluster grown using the Witten-Sander model for diffusion-limited aggregation (Fig. 6). In this case the simulation was carried out on a six coordinate hexagonal lattice.

C. The Screened Growth Model

The screened growth model is closely related to the Eden model described above. However, in the Eden model each of the unoccupied perimeter sites has more or less the same growth probability ($P_{max}/P_{min} \leq C$ where C is a finite constant. The quantities $P_{max}$ and $P_{min}$ are the maximum and minimum growth probabilities) whereas in the screened growth model there is a very broad distribution of growth probabilities (a characteristic shared with the DLA model) and $P_{max}/P_{min}$ diverges algebraically with increasing cluster size [ref. 98]. In the screened growth model the growth probability ($P_i$) associated with the ith perimeter site is given by,

$$P_i \sim \prod_{j=1}^{N} e^{-A/(r_{ij})^{\epsilon}} \quad . \tag{29}$$

Here, $r_{ij}$ is the distance from the ith unoccupied site to the jth

occupied site and N is the number of occupied sites. The screened growth model is a special case of a growth model developed by Rikvold [ref. 99] in which the growth probabilities are given by,

$$P_i \sim \prod_{j=1}^{N} e^{-A/(r_{ij}^{\varepsilon})} e^{-(r_{ij}/\lambda)} \qquad (30)$$

For Rikvold's model the ratio $P_{max}/P_{min}$ is bounded and the structures generated by this model (which may be regarded as an Eden model) have a structure which is compact on all but short length scales (length scales $\leq\lambda$). Only in the limit $\lambda\to\infty$ (the screened growth model limit [ref. 100]) does the ratio $P_{max}/P_{min}$ diverge as the cluster grows larger and larger.

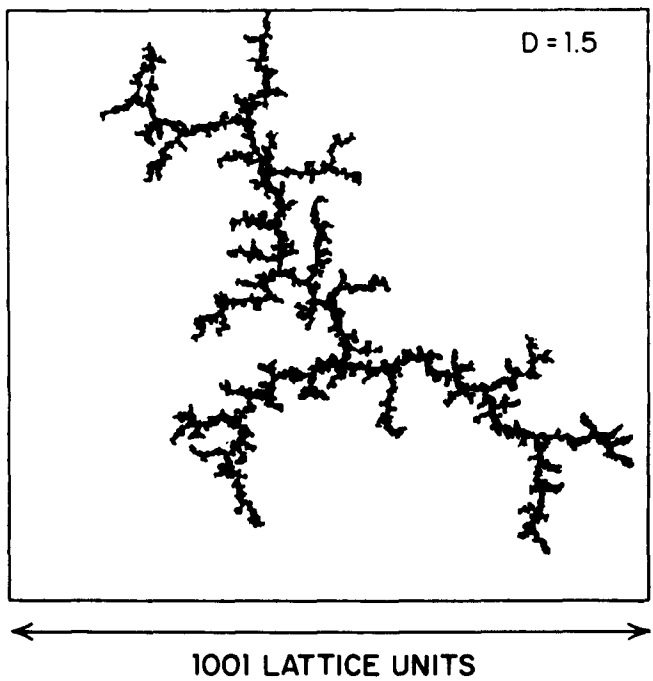


Fig. 8. A cluster of 20695 sites grown on a square lattice using a screened growth model with the parameters (A = 1.0, $\varepsilon$ = 1.5). For this model the fractal dimensionality is equal to the exponent $\varepsilon$ used in the screening function.

Figure 8 shows a cluster generated using the parameters A =

1.0, $\varepsilon = 1.5$ (for the screened growth model with $\lambda \to \infty$). Extensive computer simulations [ref. 100] show that, in for two dimensional clusters, the fractal dimension is given by $D = \varepsilon$ irrespective of the value of the parameter A. Theoretical results [refs. 101, 102] also indicate that $D = \varepsilon$. This is one of relatively few cases in which an exact theory for the fractal dimensionality associated with a non-equilibrium growth model leading to a non-trivial fractal structure exists.

Recent simulations using a cubic lattice screened growth model [ref. 103] indicate that the result $D = \varepsilon$ is valid for $d = 3$ also. Like the DLA model the screened growth model is sensitive to lattice anisotropy, but the effects of lattice anisotropy only become apparent for models in which either the anisotropy is enhanced or the noise is reduced [refs. 104-107].

Although these models do not lead to structures which closely resemble those found in most aggregation systems, the Rikvold (finite $\lambda$) model has been used by Skjeltorp [ref. 108] to describe the structures of aggregates formed from very uniformly sized polystyrene spheres (1.1 and 4.7 $\mu$ diameter) confined to an aqueous layer between two glass sheets, with treated surfaces, which are held apart by a few slightly larger spheres. The spheres were weakly stabilized with 0.1% sodium dodecyl sulfate at an ionic strength of 0.02 molar. By varying the particle sizes and ionic strengths, a variety of structures could be produced ranging from compact faceted aggregates to highly ramified structures. Skjeltorp [ref. 108] suggested that some of these structures could be understood in terms of the Eden [ref. 38] and Rikvold [ref. 99] models.

D. Colloidal Aggregation Models

A large number of computer models for colloidal aggregation have been developed during the past 30 years or so. Here we are concerned only with simple models which lead to structures with a well-defined fractal geometry. Many models of this type are based on the ballistic cluster-cluster aggregation model of Sutherland (section IVB). The most important parameter in models of this type are the way in which clusters are selected from the list of clusters and the way in which they are combined. The selection of the clusters determines how the cluster size distribution evolves. This distribution may range from one large cluster and many particles in the ballistic aggregation model of Vold (section IVA) and the DLA model of Witten and Sander to

systems in which all of the clusters have the same size (such as the hierarchical ballistic cluster-cluster aggregation model outlined in section IVB. The clusters may be brought together via random walk trajectories ($D_w = 2$), linear trajectories ($D_w = 1$) or trajectories with a fractal dimension ($D_w$) of zero (Eden growth and reaction-limited cluster-cluster aggregation, for example). Aggregation with fractal (Levy flight and Levy walk [ref. 2]) trajectories has also been explored [refs. 109, 110]. In general, a broad distribution of cluster sizes and trajectories with a low fractal dimensionality lead to the most compact (highest fractal dimensionality) clusters.

Almost identical lattice models for diffusion-limited cluster-cluster aggregation were developed simultaneously but independently by Meakin [ref. 111] and by Kolb, Botet and Jullien [ref. 112]. In this model a small fraction ($\rho_o$) of the sites on a lattice are selected at random and filled to represent the aggregating particles. Particles connected via nearest neighbor occupancy on the lattice are irreversibly combined to form clusters. As the simulation proceeds clusters (including single particles) are selected at random and moved by one lattice unit in one of the 2d possible directions (also selected at random) on a d dimensional hypercubic lattice. After a cluster has been moved, its perimeter is examined to see if any other clusters have been contacted. If two clusters do contact, they are joined permanently and their particles continue to move in concert. In the most simple version of this model clusters are selected with equal probabilities corresponding to a mass independent cluster diffusion coefficient. In general, the cluster diffusion coefficients depend on their size and/or shape. In most cases it is assumed that the cluster diffusion coefficients are given by

$$\mathcal{D}(s) \sim s^{\gamma'} , \tag{31}$$

where $\mathcal{D}(s)$ is the diffusion coefficient for clusters containing s particles or lattice sites.

A very similar model was developed earlier by Finegold [refs. 113 and 114]. However, the simulations were carried out at relatively high particle densities and no geometric scaling behavior was found. A similar diffusion-limited cluster-cluster aggregation model was also developed independently by Sunada et al. [ref. 115] to investigate aggregation kinetics.

## VI. DIFFUSION-LIMITED CLUSTER-CLUSTER AGGREGATION

In most cases colloidal aggregation involves a complex interplay between a variety of physical and chemical processes. However, at least a partial understanding of complex aggregation processes of practical importance can be developed in terms of simple limiting case models. In some cases real systems closely approximate the behavior associated with these simple models. In diffusion-limited aggregation particles and/or clusters move into close proximity with each other via random walk trajectories (Brownian motion). This picture is appropriate for aggregation in a dense fluid with an attractive particle-particle interaction potential which is larger than kT only on short length scales. If a small repulsive barrier must be overcome before a deep primary minimum is found (for irreversible aggregation), a number of collisions will be required (on average) before this barrier is crossed. Under these conditions behavior characteristic of reaction-limited aggregation will be found for small clusters with crossover to diffusion-limited aggregation at later times when the mean cluster size has grown to a sufficiently large value. However, under these conditions other processes such as settling due to gravity and convection may intervene before the diffusion-limited regime is reached.

### A. Computer Models

In the most simple models for diffusion-limited cluster-cluster aggregation clusters are brought together along random walk trajectories. It is usually assumed that once formed clusters neither break up nor change their structure. However, simple models have been developed in which structural reorganization during [refs. 116-118, section IX] or after [ref. 119] aggregation, cluster breakup [refs. 120-122] and other processes are included.

Both lattice and non-lattice models for diffusion-limited aggregation have been developed and explored. In general, lattice models are more simple and allow larger structures to be generated. These models are valuable in investigating universal scaling properties. Off-lattice models are more realistic and may give important information concerning short range structures which cannot be accurately represented in lattice models.

Figure 9 shows four stages in a small scale two dimensional simulation of cluster-cluster aggregation carried out on a square

lattice. The simulation was started by randomly occupying 2000 sites on the lattice to represent the aggregating particles. A few particles occupy adjacent sites and the system consists of 1877 clusters which move on the lattice via random walk trajectories. In this model the cluster diffusion coefficients ($\mathcal{D}(s)$) are independent of the cluster size (s) and clusters are selected randomly and moved by one lattice unit in one of the four possible directions on the lattice (also selected randomly). After each cluster has been moved its perimeter is examined for contact with other clusters. Contacting clusters (those which occupy nearest neighbor lattice sites) are permanently joined and the sites in each cluster are moved in concert.

Figure 9b shows the system at a later stage where the number of clusters has been reduced to 500 and in Figure 9c a still later stage with 125 clusters is shown. It is evident from this figure that the system is evolving toward a broad distribution of cluster sizes. At this stage a few single particle clusters remain while the large clusters contain about 50 sites. Finally Figure 9d shows the simulation at a stage in which only 10 clusters remain. The larger clusters illustrate the ramified fractal geometry which is characteristic of this model. Very similar simulations have been carried out using an off-lattice model for cluster-cluster aggregation [ref. 123].

Models very similar to those developed by Sutherland for ballistic cluster-cluster aggregation (section IVA) can also be used to provide a realistic representation of diffusion-limited cluster-cluster aggregation. In this model pairs of clusters of size i and j are selected at random and combined via off-lattice random walk trajectories if $X<K(i,j)/K_{max}$ where X is a random number uniformly distributed over the range $0<X<1$, K(i,j) is the element of the reaction kernel corresponding to clusters of size i and j and $K_{max}$ is the maximum value of K for any pair of clusters in the system. For diffusion-limited cluster-cluster aggregation, K(i,j) has the form [ref. 124],

$$K(i,j) \sim (i^{1/D}+j^{1/D})(i^{-1/D}+j^{-1/D}) \quad . \tag{32}$$

Figure 10 shows a cluster generated by a three-dimensional off-lattice model with a constant reaction kernel (K(i,j) = 1). Since this is a reasonably good approximation to the reaction kernel given in Equation (30) (except for reactions between very small and very large clusters) we expect that the structure of the aggregate will be very similar to that which would have been

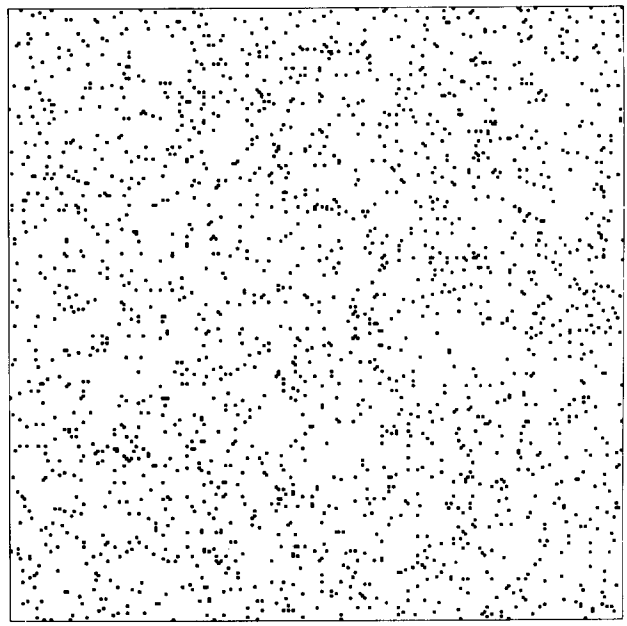

Fig. 9a. **D(s) ~ $S^0$, N = 1877, t = 0**

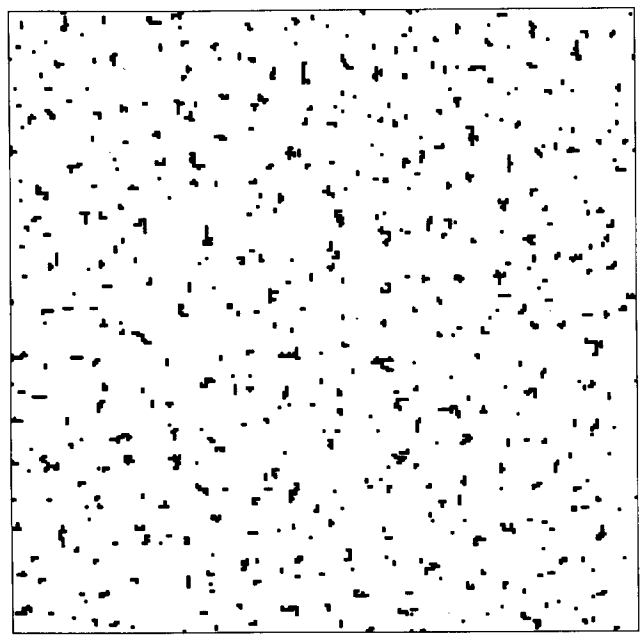

Fig. 9b. **D(s) ~ $S^0$, N = 500, t = 70**

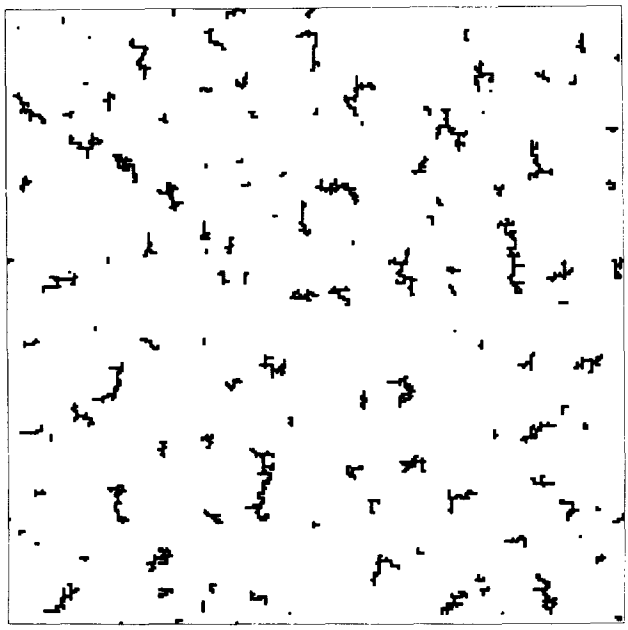

Fig. 9c. $D(s) \sim S^0$, N = 125, t = 356

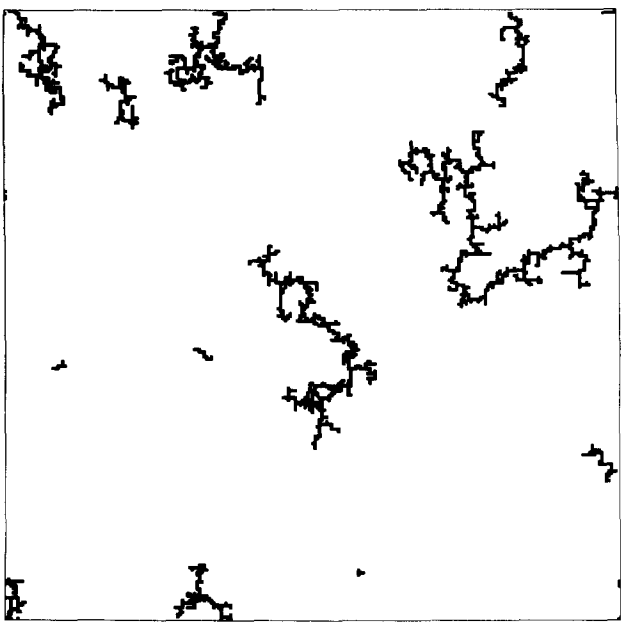

Fig. 9d. $D(s) \sim S^0$, N = 10, t = 2571

Fig. 9. Four stages in a small scale simulation of diffusion-limited cluster-cluster aggregations carried out on a square lattice.

obtained using the correct reaction kernel Equation (32)). In fact for this model the fractal dimensionality is quite (but not completely) insensitive to the reaction kernel providing that the cluster size distribution does not become too broad. From three-dimensional simulations a value of 1.80 is found for D using a constant reaction kernel [ref. 118] and 1.78 from a hierarchical model. The value obtained using the kernel in Equation (32) should lie between these two values. Consequently, it is reasonable to compare the simulated cluster shown in Figure 10 with the gold particle aggregate shown in Figure 1. Both aggregates contain about the same number of particles.

B. Aggregation Kinetics

The model illustrated in Figure 9 can easily be made time dependent. Each time a cluster is randomly selected and moved, the time is incremented by 1/N where N is the number of clusters in the system. In the more general case in which $\mathcal{D}(s)$ depends on the cluster size s clusters are selected at random but moved only if $x<\mathcal{D}(s)/\mathcal{D}_{max}$ where $\mathcal{D}_{max}$ is the maximum diffusion coefficient of any of the clusters in the system. In this model a realistic time scale can be introduced by incrementing the time by $1/(N\,\mathcal{D}_{max})$ each time a cluster is selected (whether or not it is actually moved) [refs. 125-128]. The time scale generated in this fashion is in units of the average time required to move a single particle by one lattice unit.

Using simulations of this type, it is possible to investigate the kinetics of cluster-cluster aggregation and explore the reaction kernel K(i,j) by measuring the number of clusters of size i and j and the rate at which they combine to form clusters of size i+j. Using this approach, Ziff et al. [ref. 124] shows that the effective reaction kernel for cluster-cluster aggregation simulations carried out at low particle densities is consistent with the form

$$K(i,j) \sim (i^{1/D}+j^{1/D})\,(i^{\gamma'}+j^{\gamma'}) \quad , \tag{33}$$

or

$$K(i,j) \sim (r_i+r_j)\,(\mathcal{D}_i+\mathcal{D}_j) \quad , \tag{34}$$

where $r_i$ is the mean radius for clusters of size i and $\mathcal{D}_i$ is their diffusion coefficient.

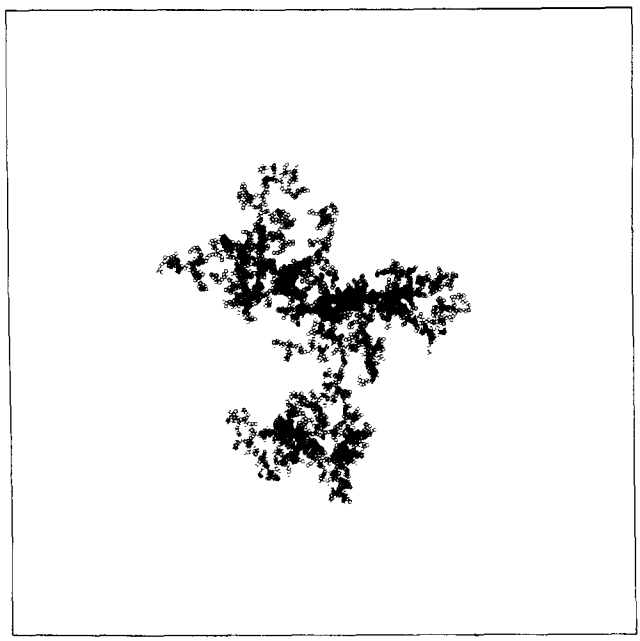


Fig. 10a.

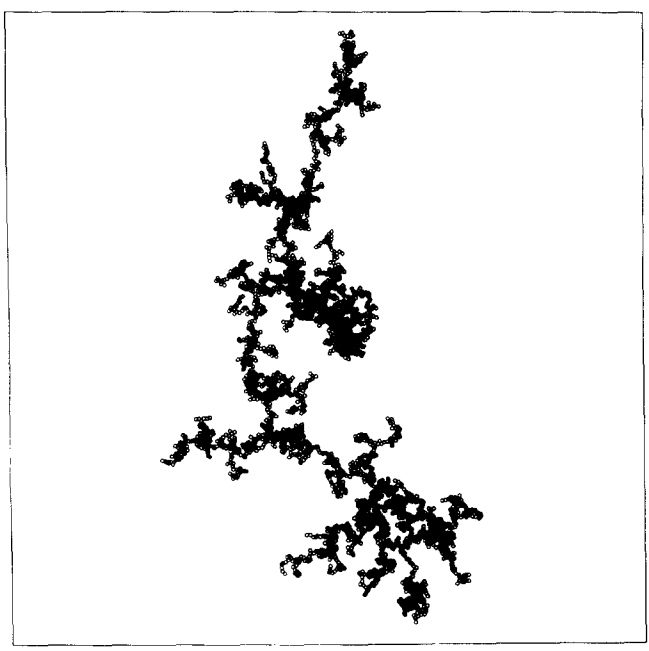


Fig. 10b.

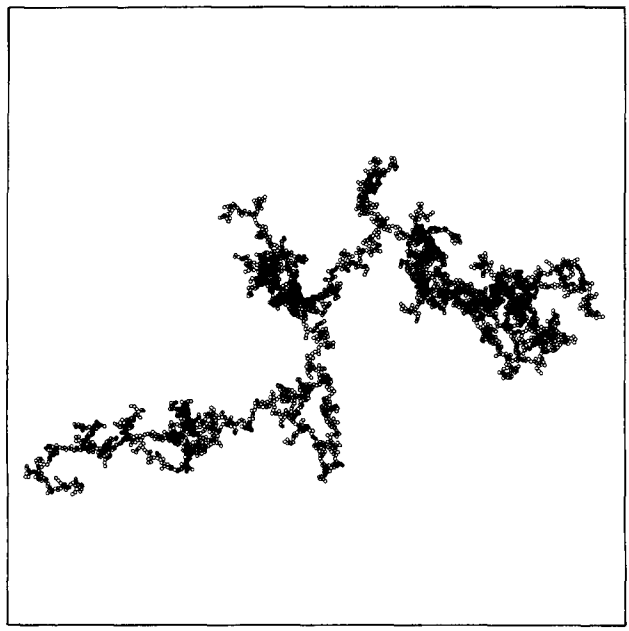


Fig. 10c.

Fig. 10. Three mutually perpendicular projections of an aggregate generated by a three-dimensional off-lattice diffusion-limited cluster-cluster aggregation model. In this simulation a constant (cluster size independent) reaction kernel was used.

Figure 11a shows cluster size distributions ($N_s(t)$ the number of clusters of size s at time t) for diffusion-limited cluster-cluster aggregation. The results obtained were from simulations of the evolution of the cluster size distribution carried out using the reaction kernel given in Equation (32). In these simulations only the cluster sizes are needed (there is no need to store the structure of the clusters). The simulation is started with $N_o$ particles of mass 1. As the simulation proceeds, particles of mass i and j are selected randomly from a list of particles and combined to form a particle of size i+j if $X<K(i,j)/K_{max}$ (where X is a random number in the range $0<X<1$) which is returned to the list. If $X \geq K(i,j)/K_{max}$ both particles are returned to the list. Each time a pair of particles is selected from the list (whether or not they are combined) the time is incremented by $1/(K_{max} N^2)$. Figure 11b shows the results

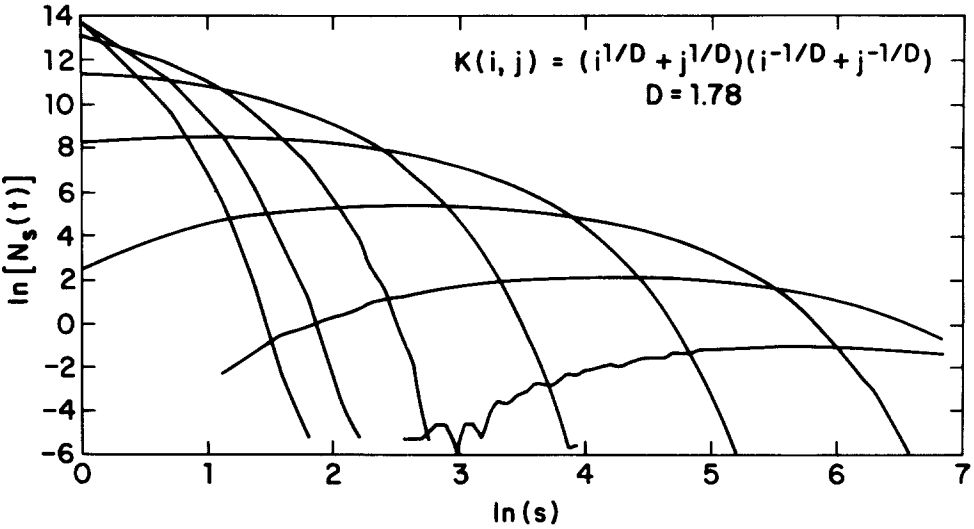


Fig. 11a.

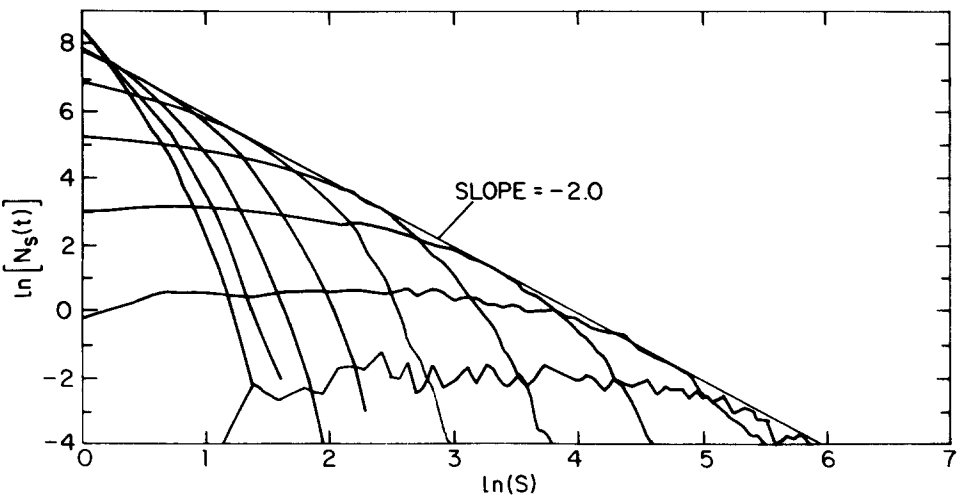


Fig. 11b.

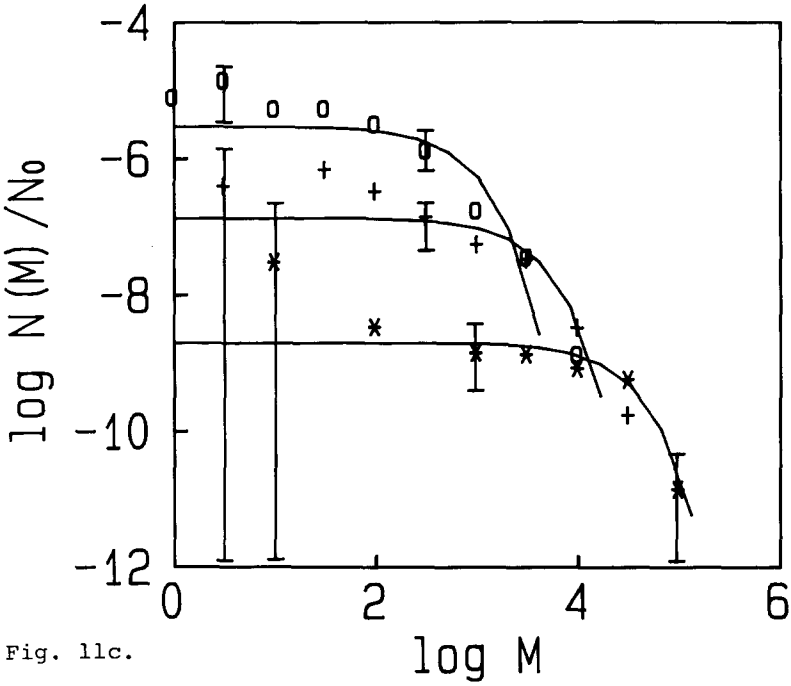


Fig. 11c.

Fig. 11. Cluster size distributions for three-dimensional diffusion-limited cluster-cluster aggregation. Figure 11a shows time dependent cluster size distributions ($N_s(t)$) obtained at several stages during the simulations carried out using the reaction kernel given in Equation (30) with a fractal dimensionality of 1.78. The results from 200 simulations each starting with $10^6$ "particles" of equal mass were used to obtain Figure 11a. Figure 11b was obtained from simulations carried out using 5,000 sites (to represent particles) on $133^3$ site cubic lattices with periodic boundary conditions. In these simulations it was assumed that $D(s) \sim s^{\gamma}$ with a value of -1/D (-0.54) for $\gamma'$. Figure 11c shows results obtained from the fast aggregation of colloidal gold. Figure 11c was provided by D. A. Weitz and is reproduced from ref. 129.

obtained from three dimensional simulations of diffusion limited cluster-cluster aggregation carried out on a cubic lattice (using an algorithm similar to that illustrated in Figure 9). The results shown in Figure 11c were obtained by Weitz et al. [ref. 129] from experimental studies on the aggregation of gold colloids under fast aggregation conditions. In all three cases the cluster size distribution evolves into a broad hump. For a constant reaction kernel the cluster size distribution would be flat with a cut-off at large cluster sizes. Small clusters are

depleted in diffusion-limited cluster aggregations because of the large size of the elements of the reaction kernels which are far off diagonal

$$K(i,j) = i^{1/D}.j^{-1/D} \text{ for } i>>j \quad (35)$$

or

$$K(i,j) \sim (i/j)^{1/D} \quad . \quad (36)$$

Analytical solutions for the Smoluchowski equation have been obtained for a variety of different reaction kernels. In most cases these reaction kernels are simple homogeneous functions of i and j which satisfy the simple scaling relationships

$$K(ai, aj) \sim a^{\lambda'}K(i,j) \quad (37)$$

and

$$K(i,j) \sim i^{\mu}j^{\nu} \text{ for } j>>i \quad . \quad (38)$$

The exponents $\lambda'$, $\mu$ and $\nu$ are related by $\lambda' = \mu+\nu$. For diffusion-limited cluster-cluster aggregation, $\lambda' = 0$ and $\nu = 1/D$.

Even in cases where the Smoluchowski equation cannot be solved analytically, it is often possible to obtain important information from the scaling properties of the reaction kernel. For example, for the case of non-gelling systems ($\lambda'<1$) the asymptotic ($t\to\infty$) growth of the mean cluster size, S(t), is given by

$$S(t) \sim t^{z} \quad , \quad (39)$$

where $z = 1/(1-\lambda')$. Here S(t) is defined as

$$S(t) = \sum_{s=1}^{\infty} s^2 N_s(t) / \sum_{s=1}^{\infty} sN_s(t) \quad . \quad (40)$$

For diffusion-limited cluster-cluster aggregation $\lambda = 0$ and we expect that $S(t) \sim t$ which is in good agreement with simulation results, numerical solutions to the Smoluckowski equation and experimental results.

For non-gelling homogeneous reaction kernels, three basic classes of behavior have been identified [refs. 130-132]. For class I kernels $\mu>0$ and the largest elements of K(i,j) are found for large values of both i and j. Under these conditions a power law cluster size distribution evolves

$$N_s(t) \sim s^{-\tau} \quad . \quad (41)$$

The value of the exponent $\tau$ is given by $\tau = 1+\lambda$ . For class II, $\mu = 0$ and the asymptotic behavior depends on the details of the reaction kernel. For class III, $\mu<0$. The largest value of K(i,j) corresponds to reactions between large and small clusters.

Under these conditions a peaked cluster size distribution evolves with few very small or very large clusters. Both the mean cluster size and the peak in the cluster size distribution grow asymptotically according to Equation (39).

C. Experimental Realizations

Perhaps the closest approach to the limiting conditions associated with the diffusion-limited cluster-cluster aggregation model is provided by the fast aggregation of a small metal particle in a dense fluid. The aggregation of small metal particles in a dense gas by Forrest and Witten [ref. 133] provided the first well established example of fractal geometry in an aggregated system. This work motivated the development of the diffusion-limited particle-cluster aggregation model by Witten and Sander [ref. 27] which in turn stimulated most of the work presented in this review.

The most extensively studied experimental example of diffusion-limited cluster-cluster aggregation is provided by the aggregation of colloidal gold. Figure 1 shows an electron micrograph of an aggregate consisting of small (about 150Å diameter) gold particles. This aggregate was prepared by adding pyridine to a gold particle dispersion stabilized by the partially screened electrostatic interaction between the particles resulting from ions adsorbed on their surfaces. A fractal dimensionality of about 1.75 was obtained by analyzing micrographs such as that shown in Figure 1. An independent determination of the fractal dimensionality ($D = 1.77 \pm 0.05$) was obtained from small angle light scattering experiments. For a fractal structure the structure factor ($S(k)$) is given by Equation (23) so that D can be determined from $S(k)$.

Similar results ($D \simeq 1.7 \pm 0.2$) have been obtained by Shonauer and Kreibig [ref. 134] by adding gelatin to gold particles stabilized by a small amount of gelatin. This system seems to be more complex than that studied by Weitz et al. and the aggregates are much smaller.

Fractal dimensionalities of about 1.75 have also been found for the fast aggregation of silica colloids (Ludox®) consisting of particles with a diameter of about 70Å [ref. 135].

In some cases fractal dimensions smaller than those obtained from the diffusion-limited cluster-cluster aggregation model have been found under fast aggregation conditions. For example, a

fractal dimensionality of 1.20±0.015 was found by Hurd and Schaefer [ref. 136] for the aggregation of silica microspheres confined to an air/water interface. This value is significantly smaller than that associated with two dimensional diffusion-limited cluster-cluster aggregation (≃1.43). It seems likely that such small fractal dimensionalities are a result of long range attractive interactions [refs. 136-139].

## VII. BALLISTIC CLUSTER-CLUSTER AGGREGATION

The trajectories followed by small particles or aggregates in a dense fluid can be adequately represented by a random walk with a fractal dimensionality of 2. However, in a gas at low pressures particles or clusters follow paths which do not change direction on length scales comparable to their sizes. Since the masses of even quite small particles are many orders of magnitude larger than those of gas molecules they do not change direction after each collision with a gas molecule. Instead many collisions are required to change significantly the direction in which a particle is moving. For this reason, the free molecular or high Knudsen number limit approximation can be applied to small particles and their aggregates even at quite high pressures. Under these conditions ballistic aggregation models can be used to simulate the formation of particle clusters and flocs.

### A. Computer Models

Most models for ballistic cluster-cluster aggregation are based on the Sutherland model [refs. 71-73] described in section IVB. For the case of ballistic aggregation in a low density gas, the reaction kernel is given by

$$K(i,j) = \sigma(i,j)\ ((i+j)/ij)^{1/2} \quad . \tag{42}$$

The first term on the left hand side of Equation (42) represents the geometric cross section for clusters of sizes i and j and the second term is obtained from the velocity distributions for clusters of sizes i and j. Here we assume that the clusters act like large molecules and that their velocities are given by the kinetic theory of gases [ref. 140]. An upper limit for the collision cross section ($\sigma(i,j)$) is given by

$$Q(i,j) = (R_i+R_j)^2 > \sigma_{ij} \quad , \tag{43}$$

where $R_i$ and $R_j$ are the maximum radii of the two clusters.

To simulate ballistic aggregation under these conditions pairs of clusters are selected randomly from the list of

clusters. A random number (X) uniformly distributed over the range $0<X<1$ is then generated and the clusters are returned to the list if

$$X>P(i,j)/P_{max} \quad . \tag{44}$$

Here, $P(i,j)$ is given by

$$P(i,j) = (R_i+R_j)^2((i+j)/ij)^{1/2} \tag{45}$$

and $P_{max}$ is the maximum value of $P(i,j)$ for any pair of clusters in the list. If the clusters are not returned to the list, they are rotated to random orientations and one of the clusters is "fired" at the other along a linear trajectory with an impact parameter randomly selected from a circle with a radius of $(R_i+R_j)$. If this brings the two clusters into contact with each other, they are irreversibly combined at the point of first contact. If the two clusters miss each other, they are returned to the list and another pair of clusters is selected.

Figure 12 shows a cluster of 10,700 particles generated using this model. The simulation was started out with 100,000 particles and the procedure described above was repeated until the size of the largest cluster exceeded 10,000 particles.

Figure 13 shows the dependence of $\ln(R_g/s^{1/2})$ on $\ln(s)$ obtained from 32 simulations each starting with 200,000 particles. These simulations were continued until the maximum cluster size exceeded 10,000. From a least squares fit of a straight line to the dependence of $\ln(R_g)$ on $\ln(s)$ for clusters in the size range $200\lesssim s\lesssim 9{,}000$ a radius of gyration exponent ($\beta$) of 0.513 was obtained and the corresponding fractal dimensionality $D_\beta$ has a value of 1.95 [ref. 76]. Here the statistical uncertainty is substantially smaller than 0.01. However, finite size effects may result in a larger systematic error. For aggregates with a fractal dimensionality smaller than 2.0, we expect that the area of a projection of the cluster onto a plane will in the asymptotic limit $s\to\infty$ be directly proportional to s

$$\sigma(s) \sim s \quad . \tag{46}$$

However, since D is quite close to 2.0 for ballistic cluster-cluster aggregation, quite large corrections to this asymptotic behavior are also expected. Figure 14 shows the dependence of $\ln(\sigma/s)$ on s obtained from nine simulations in which clusters containing up to 10,000 particles were generated starting with 200,000 particles in each simulation [ref. 76]. After each of the intermediate clusters was generated, it was

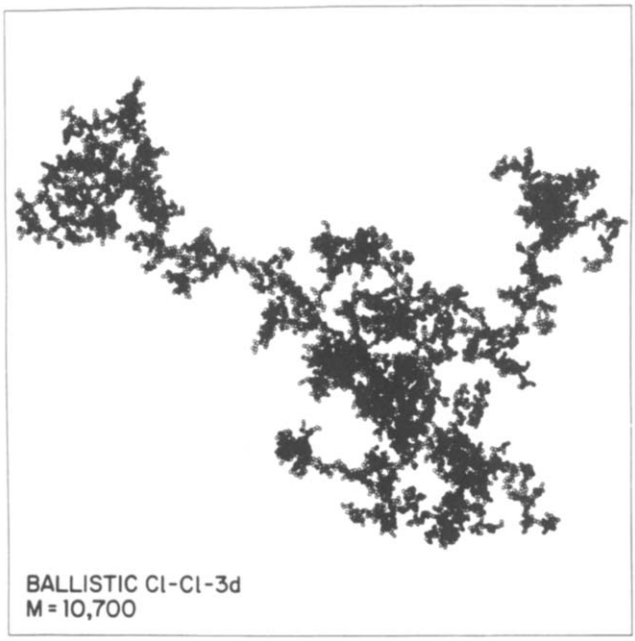


Fig. 12a.

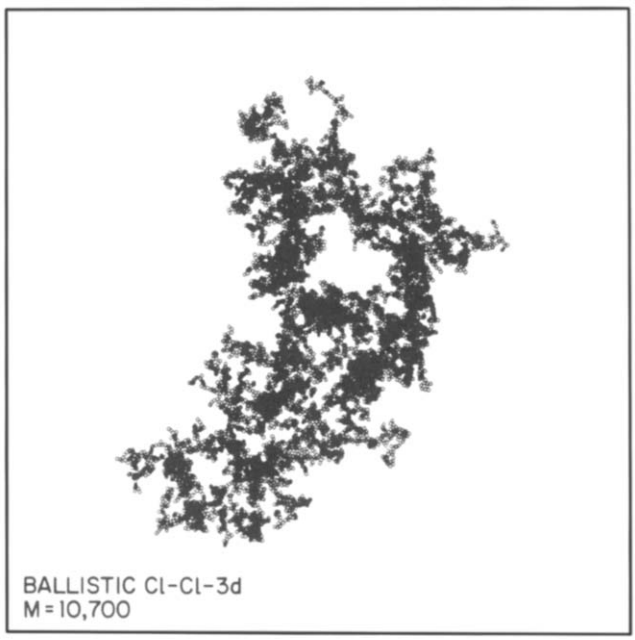


Fig. 12b.

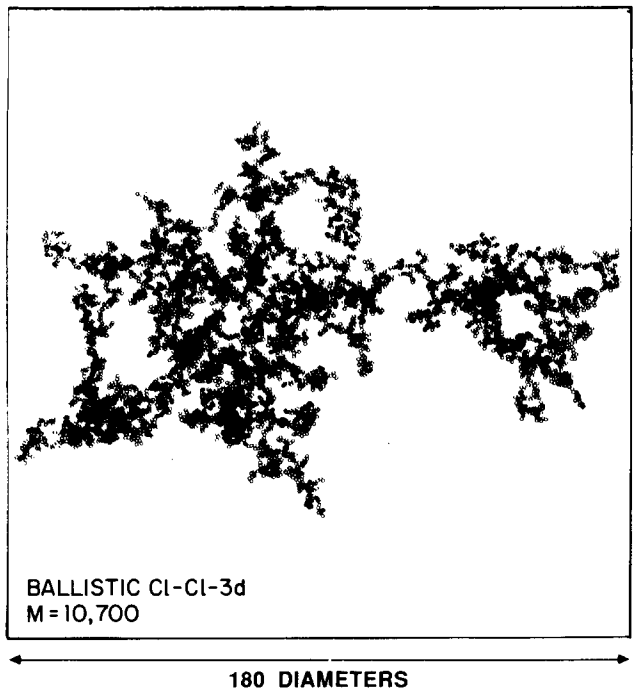


Fig. 12c.

Fig. 12. Three mutually perpendicular projections of a cluster generated using a three-dimensional off-lattice model for ballistic cluster-cluster aggregation.

projected onto 3 mutually perpendicular planes and the area of each of these projections was estimated by picking 5s points at random in a circle of radius $R_{max}$. If k of these points are in the region containing the projection, then an estimate of the cluster area is given by

$$\sigma = k\pi R_{max}^2/5s \quad . \tag{47}$$

Figure 14 shows that the size dependence of the cluster cross section can be fit quite well by the form

$$\sigma(s) = As + Bs^{\eta} \quad , \tag{48}$$

where the coefficients A and B have values of 0.264 and 0.519 respectively and the exponent $\eta$ has a value of 0.825. The dependence of $\sigma(s)$ on s was also fitted to the more general form

$$\sigma = As^{\nu'} + Bs^{\eta} \quad , \tag{49}$$

and coefficients A and B were found to have values of 0.554 and 0.264 respectively while the exponents $\nu'$ and $\eta$ were found to have

values of 0.952 and 0.644 respectively. Although the value obtained for the exponent $\nu'$ is not exactly 1.0, it is sufficiently close to 1.0 to be consistent with the idea that $\sigma \sim s$ in the large size limit in view of the uncertainties associated with a four parameter fit.

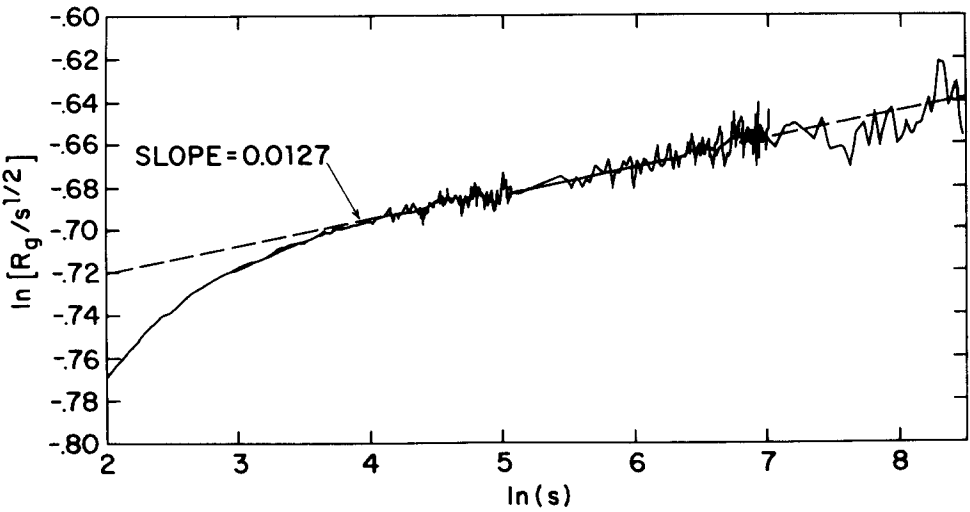


Fig. 13. Dependence of $\ln(R_g/s^{1/2})$ on $\ln(s)$ for clusters generated from the same three-dimensional off-lattice model for ballistic cluster-cluster aggregates which was used to obtain Figure 12.

The dependence of $\sigma$ on s is important in developing a better understanding of the optical and aerodynamic transport properties of aggregates. These properties play an important role in processes such as combustion, air and water pollution and the aggregation process itself. They are also important in the use of aggregated systems in paints, smoke screens and other applications.

B. Aggregation Kinetics

The model described above can be made time dependent by incrementing the time by $1/(N^2 P_{max})$ each time a pair of clusters is selected from the list (whether or not they are actually fired at each other or contact if they are fired). Figure 15 shows the

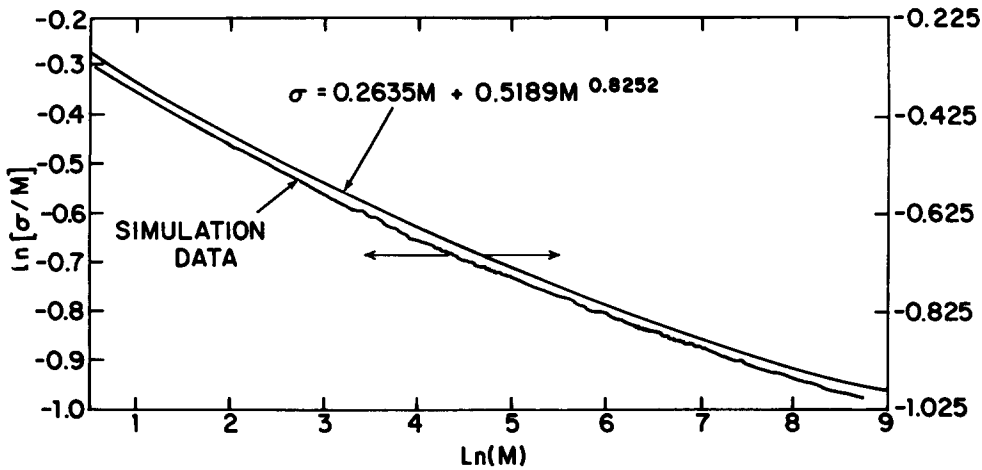


Fig. 14. Dependence of ln(σ/s) on ln(s) for simulated three dimensional ballistic aggregates. Here σ is the projected area (onto a plane) and s is the cluster size.

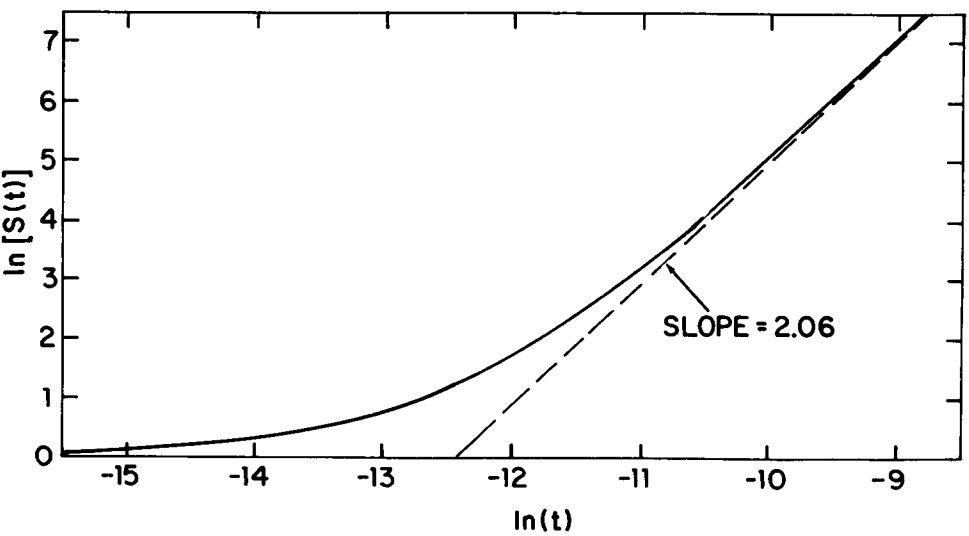


Fig. 15. Time dependence of the mean cluster site (S - Equation (40)) obtained from three-dimensional off-lattice ballistic cluster-cluster aggregation simulations. In these simulations the cluster velocity distributions were assumed to be given by the kinetic theory of gases.

dependence of the mean cluster size (S(t) - Equation (38)) on this time obtained from 32 simulations in which 200,000 particles were used. Figure 15 shows a power law growth in the mean cluster size (Equation (39)) with a value of about 2.05 for the exponent z.

For clusters of comparable size the reaction kernel is given by

$$K(i,j) \sim (i^{1/D}+j^{1/D})^2 \ (i+j/ij)^{1/2} \qquad (50)$$

so that the exponent $\lambda'$ in equation (37) is given by

$$\lambda' = 2/D - 1/2 \qquad (51)$$

and a value of $1/(1-\lambda')$ or 2.108 (for D = 1.95) is expected for z. The value obtained for z from the simulations is in quite good agreement with this value.

Figure 16a shows the cluster size distribution ($N_s(t)$) obtained at several stages during these simulations. This distribution exhibits a quite broad peak but the size distribution is narrower than that associated with 3d diffusion-limited cluster-cluster aggregation.

For clusters of very much different sizes (i>>j) the small clusters may pass right through the holes in the large clusters and equation (45) is no longer valid. Simple scaling ideas [ref. 135] based on the concepts of fractal geometry [ref. 2] indicate

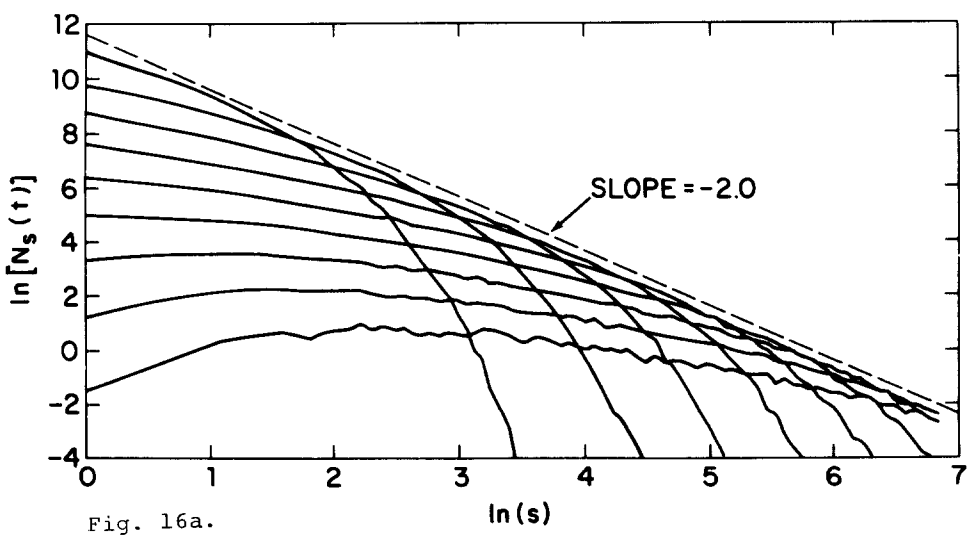


Fig. 16a.

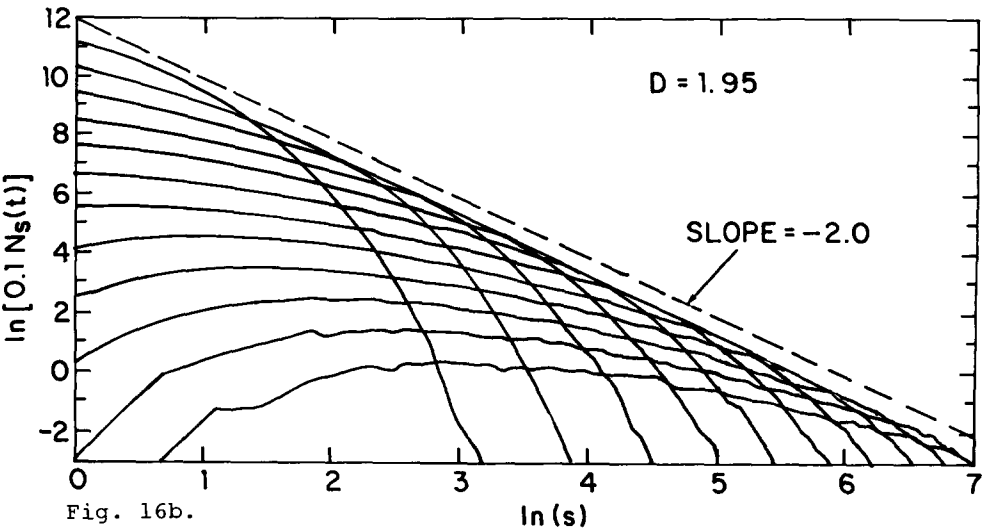


Fig. 16b.

Fig. 16. Cluster size distributions ($N_s(t)$) obtained from three dimensional simulations of ballistic cluster-cluster aggregation. Figure 16a shows some results obtained from off-lattice simulations in which the actual cross sections between pairs of clusters were used (i.e., collisions were simulated) and the cluster-velocity distribution was assumed to be given by the kinetic theory of gases. These results were obtained from 32 simulations each starting with 200,000 particles. Figure 16b shows the results obtained using the approximate reaction kernel given in equation (50). In this case the results from 6 simulations are shown. In these simulations $2 \times 10^6$ particles were used. In Figure 16b $\ln(0.1\ N_s(t))$ has been plotted so that the two parts of the figure can be directly compared.

that

$$\sigma(i,j) \sim j^{(2/D-1)} i \qquad \text{for } i \gg j \ . \qquad (52)$$

Figure 16b shows the cluster size distributions ($N_s(t)$) obtained from simulation of the aggregation kinetics using the reaction kernel given in equation (50). These simulations were carried out using the procedures described in section VIb. Although equation (50) is not valid for clusters of very disparate sizes, the results shown in Figure 16a are expected to be reasonably accurate since the cluster size distribution is distinctly peaked and collisions involving very small and very large clusters are relatively rare.

C. Experimental Realizations

Several examples of cluster-cluster aggregations have been studied under conditions which approximate those associated with

the ballistic aggregation model. Samson, Mulholland and Gentry [ref. 141] have studied the structure of soot aggregates formed by the combustion of acetylene in a coannular diffusion burner. Under the conditions of these experiments (high temperatures and small particle sizes (about 20-30 nm)) the relaxation time for the aggregate trajectories are large compared to the time required to move by the aggregate diameter (at least for small aggregates) and the aggregation takes place near to the high Knudsen number or free-molecular limit. Effective fractal dimensionalities of 1.5-1.6 were obtained for small aggregates ($<0.1$ μm diameter). For larger aggregates (5.5-12 μm) an effective fractal dimensionality of about 1.82 was found and for cluster sizes greater than 12 μm the effective fractal dimensionality was about 0.1 larger (1.90-1.95). These results are in reasonably good agreement with computer simulation results obtained from the ballistic cluster-cluster aggregation model for which the effective fractal dimensionality increases with increasing cluster size and approaches a limiting value of about 1.95 as $s \to \infty$.

Figure 17 shows one of the large aggregates obtained by Samson et al.

Hurd, Schaefer and Martin [ref. 142] used light and neutron scattering to investigate the structures of several types of fumed silica aggregates. In these aggregates the primary particle size is about 30 nm (diameter). At intermediate length scales (100-1000Å) the effective fractal dimensionality was found to lie in the range 1.7-2.0. The cluster radii of gyration were quite large (3,000-10,000Å). Under these conditions the aggregation process is probably ballistic at early stages crossing over to diffusion-limited aggregation at late stages as the cluster size exceeds the correlation length of the trajectory. The fumed silica aggregates used in this work were obtained by dispersing Cab-O-Sil in either 0.1% aqueous sodium lauryl sulfate or decanol using ultrasonification. These fumed silica aggregates seem to be quite robust but may be damaged by this procedure.

Tence et al. [ref. 143] have carried out experiments on the aggregation of iron particles prepared by radiofrequency induction heating an iron ingot in a cryogenic environment. The iron particle aggregates consist of spherical particles with

diameters ranging from about 100Å to 2000Å with a mean size of about 500Å. In this system, aggregation appears to take place at high temperatures since some of the particles seem to be welded together. From digitized images of electron micrographs a fractal dimensionality of $1.90 \pm 0.1$ was obtained. Several different methods of estimating D were used. In one of these the aggregate mass was obtained by integrating the intensity of a dark field image over an entire aggregate and from the dependence of this mass on the overall cluster diameter the fractal dimensionality was obtained.

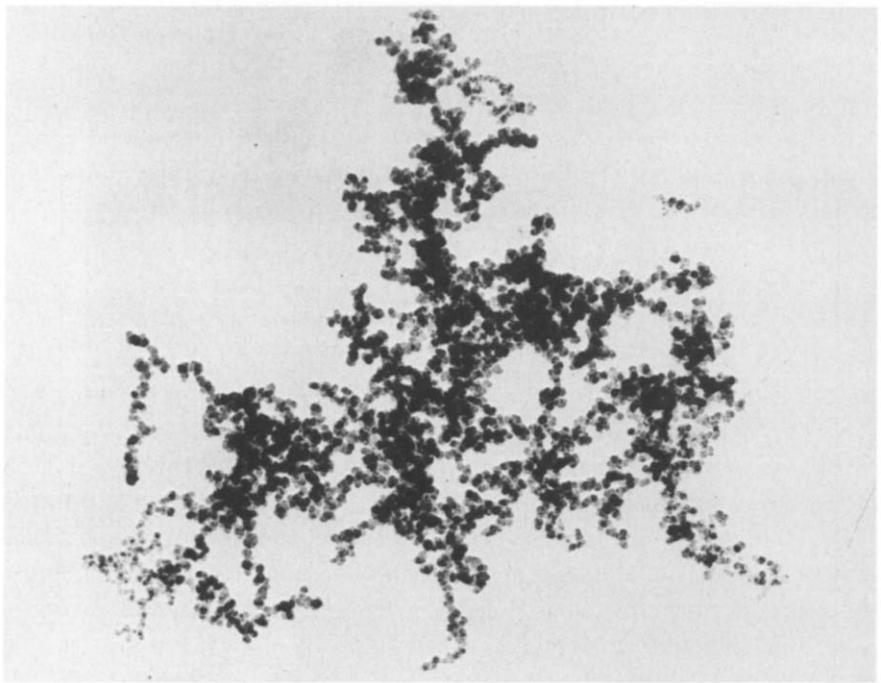

Fig. 17. Transmission electron micrograph of a soot aggregate formed by acetylene combustion. This picture was provided by G. W. Mulholland and is reproduced from Samson et al. [ref. 141].

The results of these experiments were compared with ballistic cluster-cluster aggregation simulations. Since the aggregates are quite large and the conditions under which aggregation is occurring are not well defined, we cannot be sure whether a diffusion-limited or ballistic aggregation model is the most appropriate (i.e., if the experiments are occurring under conditions in which the correlation length for the cluster

trajectories and their overall sizes are comparable). However, the measured fractal dimensionality is closer to the value expected for polydisperse ballistic aggregation (about 1.95) than for diffusion limited aggregation (about 1.80).

## VIII. REACTION LIMITED CLUSTER-CLUSTER AGGREGATION

In reaction-limited cluster-cluster aggregation many encounters between pairs of clusters are required before aggregation occurs. In the most simple aggregation models considered here it is assumed that once bonding has been established the clusters are rigid and irreversibly bound together. In some respects the reaction-limited aggregation model is more simple than the ballistic and diffusion-limited aggregation model but was not developed until quite recently.

A theoretical model for reaction-limited cluster-cluster aggregation has been proposed by Ball et al. [ref. 144]. The analysis of Ball et al. is concerned with reaction-limited aggregation under conditions where all bonding configurations between pairs of clusters have equal probabilities of being selected. They find that under these conditions the reaction kernel can be described in terms of its scaling properties

$$K(i,j) \sim ij^{\lambda'-1} \qquad \text{for } i \gg j \qquad (53)$$

$$K(i,j) \sim i^{\lambda'} \qquad \text{for } i \simeq j \qquad (54)$$

with the exponent $\lambda'$ having a value of 1 in three dimensions. Ball et al. argue that a reaction kernel with these scaling properties will lead to exponential growth in the mean cluster size (S) and a power law cluster size distribution with a value of 1.5 for the exponent $\tau$ (Equation (41)).

### A. Computer Models

One approach towards simulation of reaction-limited cluster-cluster aggregation is to use a diffusion-limited cluster-cluster aggregation model but join clusters together irreversibly with a small probability ($\sigma'$) each time they attempt to overlap. In practice, it is only possible to reduce $\sigma'$ to values of $10^{-3}$ to $10^{-4}$ in reasonably large scale simulations. However, this allows us to approach reasonably close to the reaction limited ($\sigma' \to 0$) limit. A different approach must be taken to reach the $\sigma' \to 0$ limit.

A hierarchical model for reaction-limited cluster-cluster aggregation was developed by Jullien and Kolb [refs. 145, 146]. In this model, $2^m$ particles are combined in stages so that at

each stage the clusters are all of the same size. In this lattice model all possible ways of joining pairs of clusters are found and one of these is selected at random. From simulations in which clusters containing up to 512 occupied sites were generated, effective fractal dimensionalities of 1.53±0.04, 1.98±0.04 and 2.32±0.04 were obtained for d = 2, 3 and 4.

Jullien and Kolb also measured the number of contacting configurations $C_N$ for pairs of clusters containing N particles. They found that $C_N$ depended algebraically on N according to

$$C_N \sim N^{\lambda'},$$

where the exponent $\lambda'$ had values of 0.74, 1.16 and 1.44 for d = 2, 3 and 4 respectively.

Brown and Ball [ref. 147] developed a model in which pairs of clusters are selected and placed at random on a cubic lattice. In this model the selected pairs of clusters are combined only if they are adjacent to each other but do not overlap. Depending on how the clusters are selected, the cluster size distribution may be monodisperse (as in the case in a hierarchical model) or may evolve in a natural way into a polydisperse cluster size distribution if the clusters are selected at random irrespective of their sizes. Using this model a fractal dimensionality of 1.94±0.02 was found for the monodisperse case and 2.11±0.03 for the polydisperse case in three-dimensional simulations. For d = 2, values of 1.53±0.01 and 1.59±0.01 respectively were obtained. The exponent $\lambda'$ was found to have values of 1.16±0.04 and 1.06±0.02 for the monodisperse and polydisperse three-dimensional model and 0.75±0.01 and 0.73±0.02 for the monodisperse and polydisperse two-dimensional models.

A reaction-limited reaction aggregation model proposed by Leyvraz [ref. 148] which is very closely related to the model of Brown and Ball [ref. 147] has been investigated by Meakin and Family [refs. 149, 150]. This model starts with a large number of particles. Pairs of particles are selected at random and placed in contact with each other. If the particles are contained in the same cluster, a new selection is made. If the particles are contained in different clusters, all of the particles in these clusters are moved with the selected pair of particles when they are moved into contact with each other. If the two clusters overlap, a new pair of particles is randomly selected. If no overlap is found, the two clusters are combined

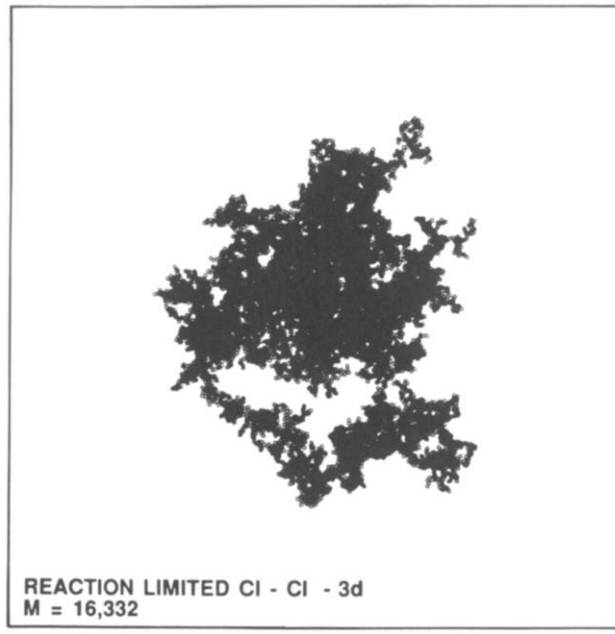


Fig. 18a.

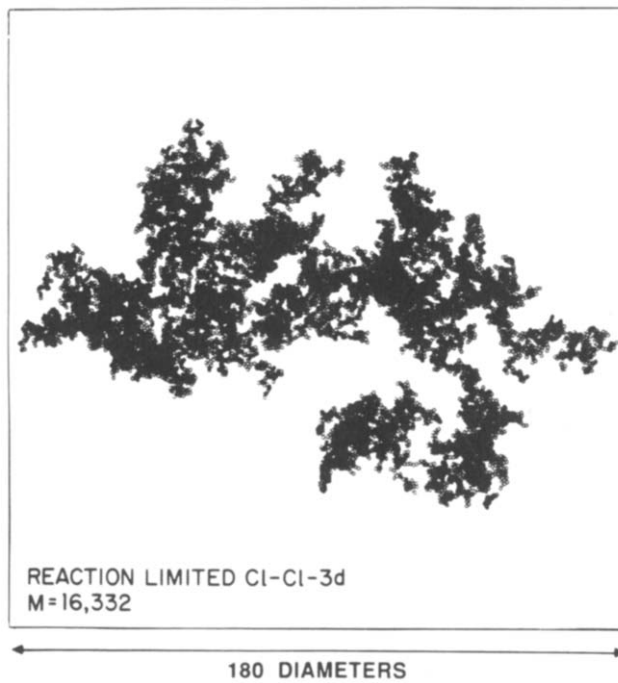


Fig. 18b.

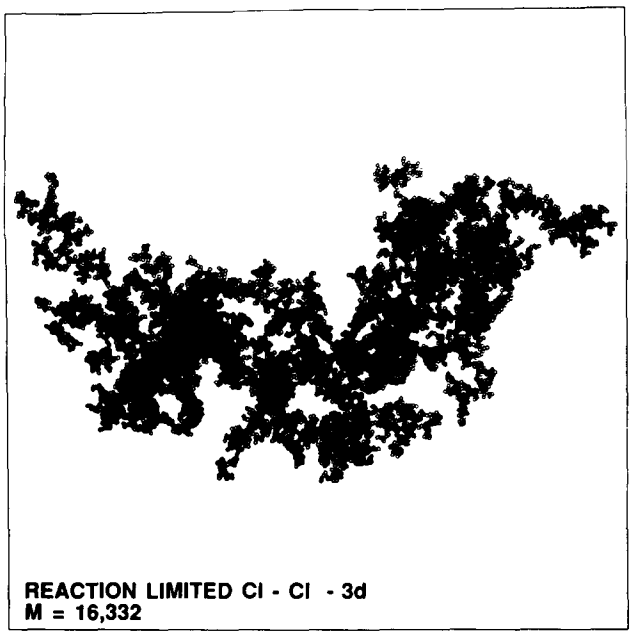


Fig. 18c.

Fig. 18. Three projections (in mutually perpendicular directions) of a cluster of 16332 particles generated by a polydisperse off-lattice model for reaction-limited aggregation.

irreversibly. Figure 18 shows a cluster of 16332 particles generated in this way. Figure 19 shows the dependence of $\ln(R_g/s^{1/2})$ on ln(s) obtained from 22 simulations. Each simulation was started with 200,000 particles and ended when the largest cluster size exceeded 3,000 particles. Both cubic lattice and off-lattice models have been investigated. The results shown in Figures 18 and 19 were obtained from the off-lattice model. From the dependence of $\ln(R_g/s^{1/2})$ on ln(s) shown in Figure 19 a fractal dimensionality ($D_\beta$) of 2.09 was obtained. The statistical uncertainty is smaller than 0.01, but since $D_\beta$ depends slightly on the maximum cluster size used in the simulations (degree of aggregation) as well as the cluster sizes used to obtain $D_\beta$, the systematic uncertainties in the asymptotic value for $D_\beta$ are almost certainly larger than 0.01. Somewhat larger values for $D_\beta$ were obtained from the lattice model.

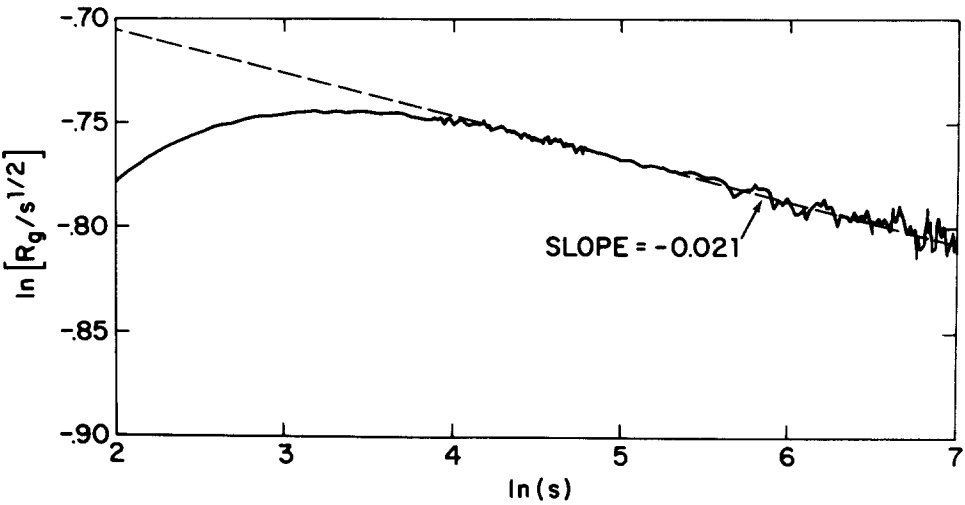


Fig. 19. Dependence of $\ln(R_g/s^{1/2})$ on ln(s) obtained from the three-dimensional off-lattice reaction-limited aggregation model.

B. Aggregation Kinetics

The kinetics of reaction-limited cluster-cluster aggregation can be simulated by increasing the time by $1/(N_o^2)$ each time a pair of clusters is selected in the model described in the last part of the previous section. Figure 20a shows the time dependence of the mean cluster size obtained from the same simulations which were used to produce the results shown in Figure 20a. In practice it is not easy to distinguish between power law growth (Equation (39)) with a large value for the exponent z, exponential growth, or gelation ($S(t) \sim (t_g - t)^{-\theta}$) where $t_g$ is a finite gel time. However, the results shown in Figure 20a do support the idea [ref. 144] that the mean cluster size grows exponentially.

Figure 20b shows the time dependence of $R_z$ (the z averaged radius) for colloidal silica (Ludox®-SM) aggregates formed under slow aggregation conditions [ref. 151]. In these experiments aggregation was initiated by titrating 0.1% Ludox®-SM samples to pH 5.5 and adding salt. A fractal dimensionality of $2.05 \pm 0.05$ was found (in good agreement with the simulation results described above) from light scattering measurements. The exponential growth which is apparent in Figure 20b is in good

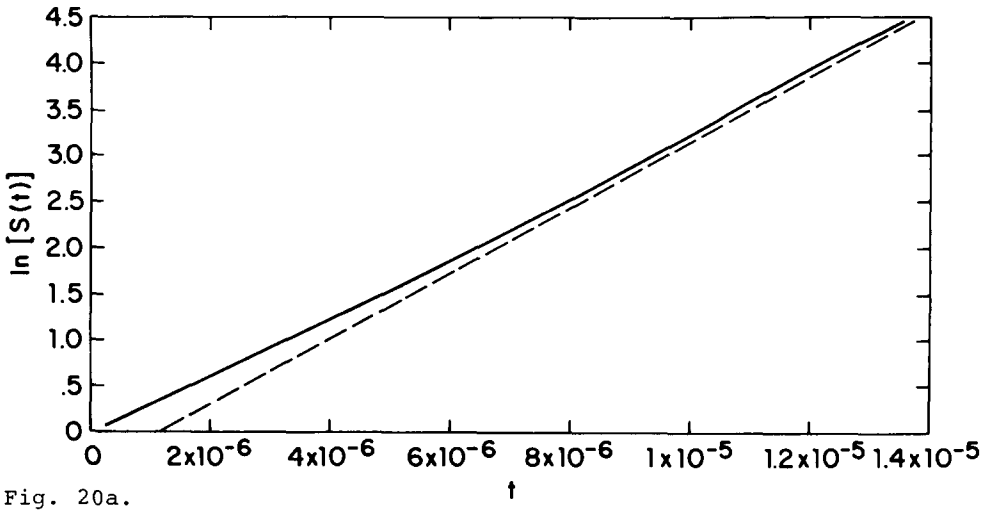


Fig. 20a.

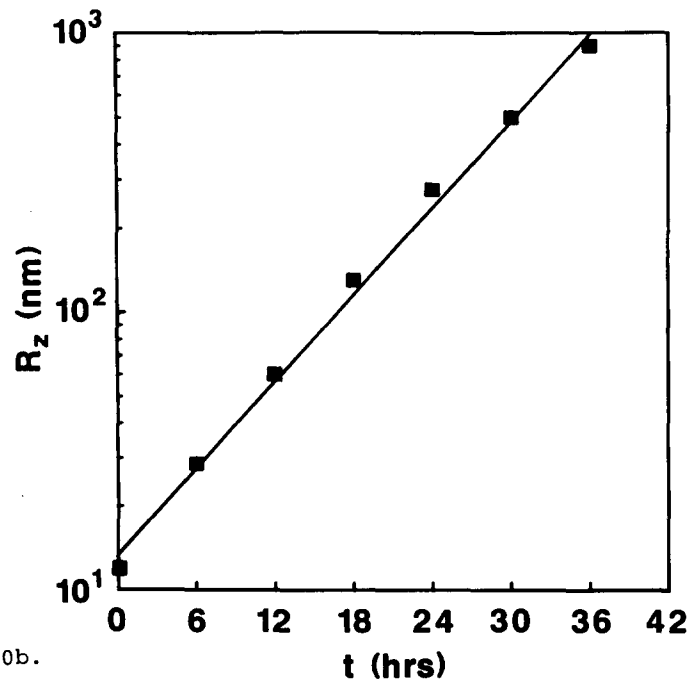


Fig. 20b.

Fig. 20. Growth of the mean cluster size in reaction-limited cluster-cluster aggregation. Figure 20a shows the dependence of ln(S) on t obtained from the three-dimensional off-lattice simulations which were used to obtain Figure 19. Figure 20b shows the time dependence of the z average cluster radius ($R_z$) found for colloidal silica aggregates (Ludox®-SM) formed under slow aggregation conditions. This figure was provided by J. E. Martin.

agreement with theory, simulation results and experimental work on other systems [refs. 152-156].

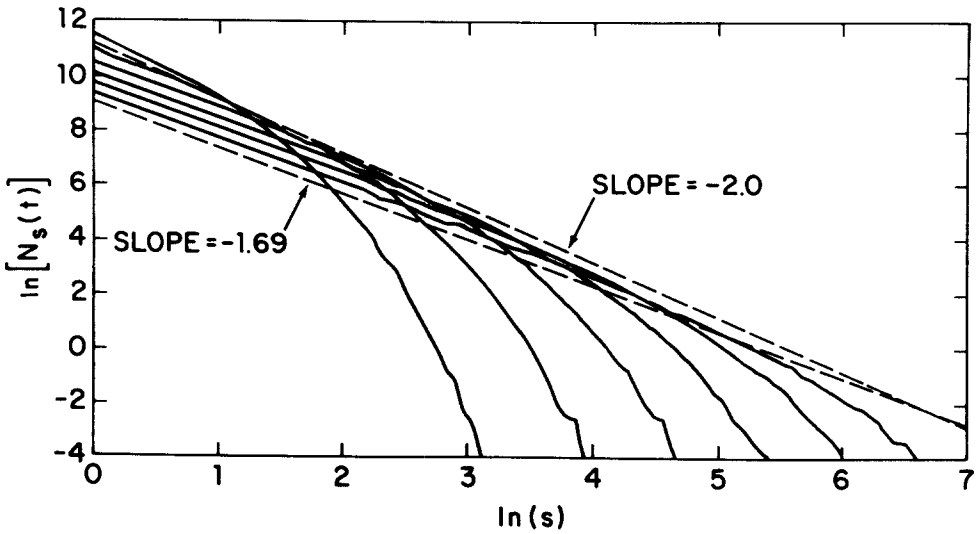


Fig. 21. Cluster size distributions obtained from the same off-lattice model for chemically-limited aggregation used to generate the results shown in Figures 19 and 20a. The cluster size distributions are shown in the stages when N has reached the values $N_o/(2)^{n/2}$ (n = 1-6). $N_o$ is the total number of particles (200,000 in this case).

Figure 21 shows cluster size distributions obtained from the simulations which were used to generate Figure 18. Here the time dependent cluster-size distribution, $N_s(t)$, is displayed at the stages where the total number of clusters has been reduced to $N_o/2^{n/2}$ for n = 1-6. Figure 21 shows that the cluster size distribution evolves towards a power law form (Equation (39)) with a cutoff at large cluster sizes. The effective value for the exponent $\tau$ in Equation (39) is about 1.7. This is somewhat larger than the value of 1.5 predicted by the theoretical arguments of Ball et al. [ref. 144] and found by Weitz et al. [ref. 153] for the slow aggregation of colloidal gold. Similarly, Von Schulthess et al. [ref. 152] have found a value of $1.40 \pm 0.15$ for $\tau$ from experimental studies of the aggregation of antigen coated polystyrene latex particles with antibody. However, values for $\tau$ close to 2.0 have been found by Martin for the slow aggregation of colloidal silica [ref. 151] and Rarity

and Pusey [ref. 154] have also found values close to 2.0 for systems undergoing slow aggregation. At the present time it is not known if these discrepancies between theory, experiments and simulation are a result of finite size and finite time corrections and statistical uncertainties or if they have a more fundamental origin. Computer simulation results indicate that the exponent $\tau$ is reduced to a value of about 1.15 if the probability that two clusters will join depends on their collision frequency rather than the amount of time which they spend near to each other [refs. 149 and 150].

C. Experimental Realizations

The results of several experimental investigations of slow aggregation kinetics under conditions which approach those assumed in reaction-limited aggregation models have been outlined in the previous section (VIIIB) on the kinetics of reaction-limited aggregation. In addition, a variety of experimental studies have been directed towards the structure of clusters formed by reaction-limited aggregation.

For example, Weitz et al. [ref. 153] have investigated the structure of gold particle aggregates formed by the addition of small amounts (about $10^{-5}$ molar) of pyridine to stabilized gold particle aggregates. Under these conditions slow aggregation occurs leading to the formation of structures such as that shown in Figure 22. If much larger amounts of pyridine ($10^{-2}$ molar) are added, a crossover is observed from slow aggregation (exponential growth of the mean cluster size) at short times to diffusion-limited aggregation (linear growth of the mean cluster size) at long times. The gold particle aggregate shown in Figure 22 should be compared to the aggregate shown in Figure 1 and the clusters generated from a three-dimensional reaction-limited aggregation model (Figure 18). Since the gold particles in the aggregate shown in Figure 22 are so small, it is possible to resolve individual gold particles to a depth of approximately three diameters. This allows the fractal dimensionality of the aggregate to be estimated from micrographs such as that shown in Figure 22 even though their fractal dimensionality is larger than 2.0 (provided the aggregates are not too large). A fractal dimensionality of $2.01 \pm 0.10$ was obtained from the dependence of the cluster mass (number of particles) on their radius from the electron micrographs. A more reliable estimate of the fractal dimensionality was obtained from *in situ* light scattering

experiments (from the shape of S(k) - Equation (23)). In this way a fractal dimensionality of 2.05±0.05 was found [ref. 153].

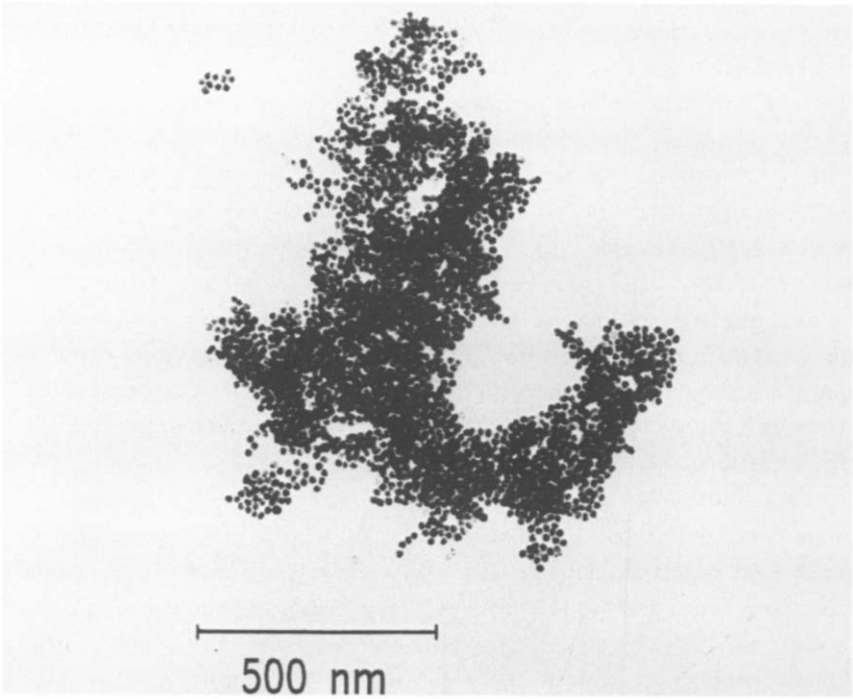


Fig. 22. Transmission electron micrograph of a gold particle aggregate formed under slow aggregation conditions. This figure was provided by D. A. Weitz and is reproduced from ref. 149. The aggregate contains about 8000 particles.

Schaefer et al. [ref. 155] have used both light and x-ray scattering to measure the fractal dimensionality of silica particle (Ludox®-SM) aggregates. In these systems aggregation was brought about by decreasing the pH to 5.5 and increasing the salt (NaCl) concentration to >0.5 molar. This procedure resulted in a slow aggregation process and after sufficiently large clusters had grown power law structure factors (Equation (21)) were found from which a fractal dimensionality of 2.12±0.05 was obtained. Although a lattice animal (see below) model was suggested, this appears to be an example of reaction-limited cluster-cluster aggregation [ref. 156].

Subsequently, Aubert and Cannell [ref. 156] found that (depending on the aggregation conditions) a fast aggregation process leading to clusters with a fractal dimensionality of

about 1.75 or slow aggregation to form clusters with a fractal dimensionality of 2.08±0.05 could be observed in the colloidal silica system. Aubert and Cannell also found that the aggregates with a fractal dimensionality of 1.75 would restructure to form aggregates with a fractal dimensionality of 2.08. Under some conditions rapid aggregation to a fractal dimensionality of 2.08±0.05 was also observed. However, this process appears to consist of rapid diffusion-limited aggregation to a fractal dimensionality of 1.75 followed by restructuring to a fractal dimensionality of 2.08.

Martin [ref. 151] has used both elastic and quasielastic light scattering to investigate the aggregation of colloidal silica at low concentrations. From static light scattering measurements on 0.1% Ludox® SM samples to which salt was added and the pH titrated to 5.5 a fractal dimensionality of 2.05±0.06 was found after 24 hours at 60°C.

## IX. OTHER PROCESSES

Aggregation in most real systems involves a wide range of physical and chemical processes including long and short range interaction (Van der Waals forces, screened electrostatic interactions, steric effects, hydrodynamic interactions, etc.), adsorption and desorption of ions and neutral species, chemical bond formation, sintering, bridging, etc. In addition, a variety of processes can occur during and after aggregation. These include structural reorganization, reversible aggregation and chemical processes. In addition, many aggregation processes involve particles with a broad range of size, shapes and compositions. The aggregating particles may also have a complex surface geometry and large heterogeneities in their surface chemistry. It is clear that incorporation of all of these (and many other) effects (such as changes in the solvent structure near to the particle surfaces) into a single model would be a formidable undertaking. In the past few years a number of attempts have been made to investigate some of the effects mentioned above by extending the very simple models discussed in sections VI to VIII. The philosophy behind most of this work has been to attempt to develop more realistic models while retaining the simplicity, reliability and tractibility of the basic models for cluster-cluster aggregation. The results of some of this work are reviewed in this section.

A. Restructuring During and After Aggregation

In many cases aggregation can be considered to proceed in two stages. In the first stage clusters move into contact with each other and are held together by relatively weak Van der Waals interactions. These weak interactions can be disrupted by thermal fluctuations, external fields or by the relative momentum of the two colliding clusters leading to fission or to structural reorganization. If the clusters remain in contact, they may become more permanently and rigidly joined as a result of processes such as sintering and the formation of metallic or covalent bonds. These considerations have motivated the development of simple cluster-cluster aggregation models in which structural readjustment is allowed after two (rigid) clusters have come into contact with each other.

Figure 23 illustrates a simple two dimensional model of this type [ref. 116]. After two clusters (cluster 1 and cluster 2) have come into contact with each other there will, in general, be only one point of contact between the two clusters. A particle at position $\underset{\sim}{C}_1$ in cluster 1 will contact a particle at position $\underset{\sim}{C}_2$ in cluster 2 where $\underset{\sim}{C}_1$ and $\underset{\sim}{C}_2$ are the positions of the centers of the two particles. In the model illustrated in Figure 22 cluster 2 is first rotated about $\underset{\sim}{C}_1$ until a second contact is established between the two clusters. If both of these contacts involve the particle at position $\underset{\sim}{C}_2$ in cluster 2, then a second rotation is possible in which cluster 1 rotates about $\underset{\sim}{C}_2$ until a third contact between the two clusters is found. The directions of the rotations used in these models can be selected in several ways. For example, the smallest rotation needed to establish a new contact can be used or the direction of rotation which will move the centers of mass of the two clusters together can be used. If the two clusters undergo rotational diffusion after they have come into contact, then the angle of rotation is selected according to

$$P(\Theta_1)/P(\Theta_2) = \Theta_2/\Theta_1 \qquad (55)$$

where $\Theta_1$ and $\Theta_2$ are the magnitudes of the two possible rotation angles which will result in a new contact. Here $P(\Theta_1)$ and $P(\Theta_2)$ are the probabilities for rotation through the angles $\Theta_1$ and $\Theta_2$ respectively. Figure 23 shows a small (512 particle) cluster generated using a two-dimensional hierarchical diffusion-limited cluster-cluster aggregation model in which restructuring was included. The smallest of the two possible angles ($\Theta_1$ and $\Theta_2$)

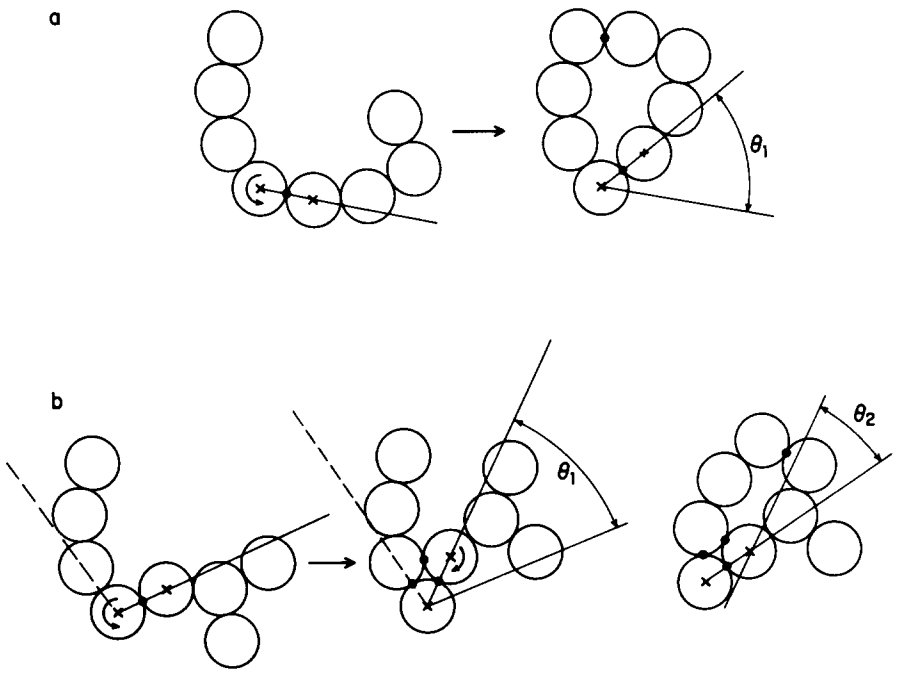


Fig. 23. A simple two-dimensional model for cluster restructuring during aggregation. Figure 23a shows the rotation of cluster 2 about the center of the contacting particle on cluster 1 to form a second bond. In this case, the second rotation of cluster 1 about the contacting particle in cluster 2 does not occur since a true loop involving bonds between two different particles on the two clusters has been formed in the first step. Figure 23b shows the rotation of cluster 2 by an angle $\theta_1$, about the center of the contacting particle in cluster 1 followed by a rotation of cluster 1 about the center of the contacting particle in cluster 2. In this case, the first rotation does not form a true loop (a loop involving 4 or more particles) and the second rotation is possible. In Figures 23a and 23b the centers of particles are indicated by crosses and new bonds are indicated by large dots.

was always selected and both stages of the restructuring process described above were carried out. For this model an effective fractal dimensionality of $1.438 \pm 0.005$ was found without restructuring. Effective fractal dimensionalities of $1.475 \pm 0.010$ and $1.485 \pm 0.015$ were found with one and two stages of restructuring respectively [ref. 116]. Similar small effects were found with the "rotational diffusion" model and for two dimensional ballistic cluster-cluster aggregation models. While the effects on the long range structure (expressed by the fractal

dimensionality) is quite small, the effect on the short length scale structure is quite important (Figure 24). A similar model for structural reorganization after aggregation is complete has also been investigated [ref. 119]. Skjeltorp [ref. 108] investigated the two dimensional aggregation of uniformly sized (1.1 μm and 4.7 μm diameter) polystyrene spheres confined to a thin layer between surface treated glass sheets separated by a few slightly larger spheres. For the larger spheres, direct visual examination indicated a structural reorganization process similar to that described above with rotation predominantly in the direction of the smallest angle needed to form a closed loop. The resulting aggregates were very similar to the simulated aggregate shown in Figure 24 and a fractal dimensionality of $1.49 \pm 0.05$ was measured. Some of the aggregates obtained by Skjeltorp are shown in Figure 25.

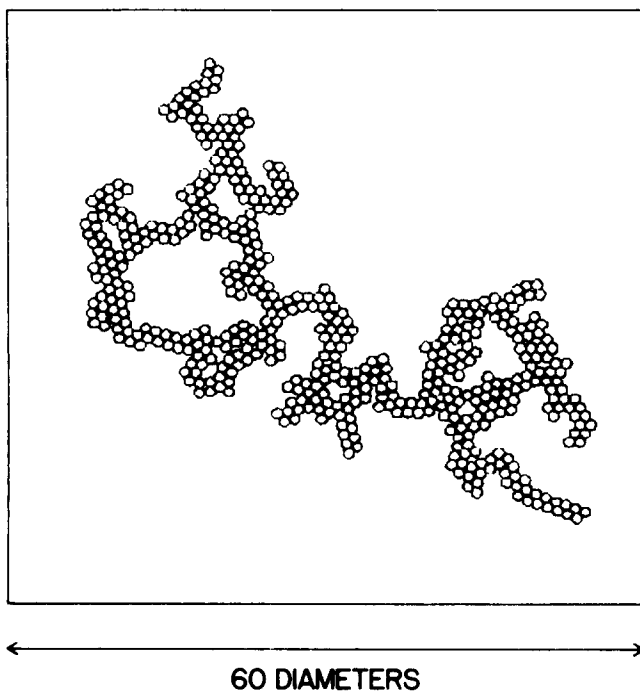


Fig. 24. A 512 particle cluster formed by two dimensional diffusion-limited cluster-cluster aggregation. Two readjusting rotations were included. For each rotation, the smallest angle was selected.

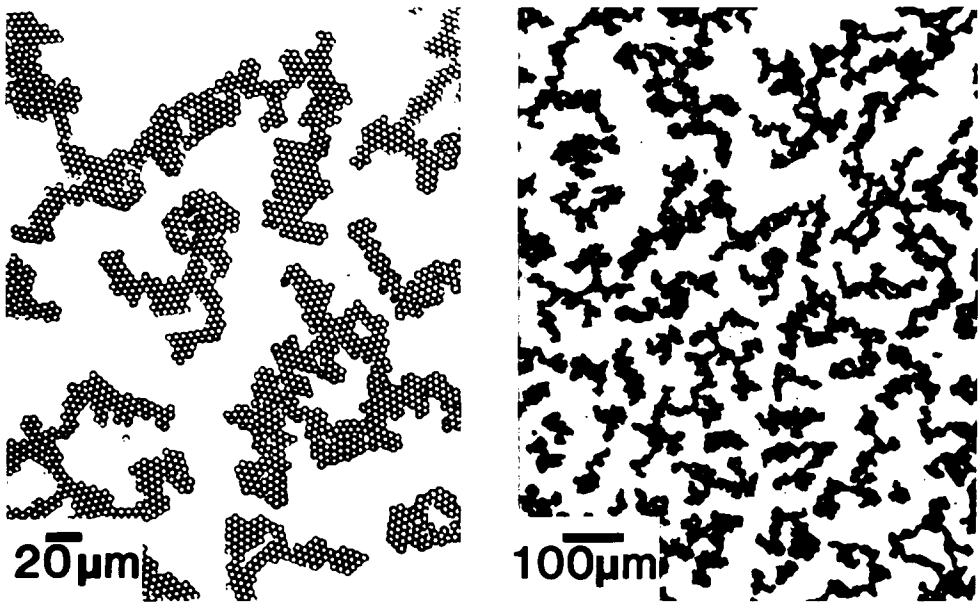


Fig. 25. Aggregation of 4.7 μm polystyrene spheres at a density of 0.14 relative to that of a close packed lattice. The aggregation was carried out in an aqueous medium confined between parallel glass sheets with treated surfaces. The glass sheets were separated by a small number of slightly larger spheres. Here aggregation is believed to be diffusion-limited and rotation of pairs of clusters about their point of contact was observed. Figures 25a and 25b show the same system on different length scales. This picture was provided by A. T. Skjeltorp.

Three dimensional models similar to the two dimensional structural readjustment models have also been developed [refs. 117, 118]. In this case, the restructuring can occur in three stages. In stage 1, cluster 2 is rotated about $\underset{\sim}{C}_1$ until a new contact is made. The direction of rotation is given by $\underset{\approx}{\Omega} = \underset{\sim}{C}_1\underset{\sim}{G}_1 \otimes \underset{\sim}{C}_2\underset{\sim}{G}_2$ where $\underset{\sim}{G}_1$ and $\underset{\sim}{G}_2$ are the positions of the centers of gravity of the two clusters and $\underset{\sim\sim}{AB}$ is a vector from $\underset{\sim}{A}$ to $\underset{\sim}{B}$ ($\underset{\sim\sim}{AB} = \underset{\sim}{B}-\underset{\sim}{A}$). If no contact is found, then the angle of rotation which will bring $\underset{\sim}{G}_1$ and $\underset{\sim}{G}_2$ closest to each other is selected. After cluster 2 has been rotated about $\underset{\sim}{C}_1$ an attempt is made to rotate cluster 1 about $\underset{\sim}{C}_2$.

At the end of stage 1 there are two contacting particles in

both clusters, $\underset{\sim}{C}_1$ and $\underset{\sim}{C}_1'$ in cluster 1, and $\underset{\sim}{C}_2$ and $\underset{\sim}{C}_2'$ in cluster 2. In the second stage of restructuring, cluster 2 is rotated about $\underset{\sim}{C}_1\underset{\sim}{C}_1'$ in the direction which will bring the centers of mass of the two clusters closer together. After this process is complete, an attempt is made to rotate cluster 2 about $\underset{\sim}{C}_2\underset{\sim}{C}_2'$. If no contact is found, the angle of rotation which minimizes $|\underset{\sim}{C}_1-\underset{\sim}{C}_2|$ is selected. In some cases further restructuring of the two rigid clusters is still possible. In stage 3 attempts are made to carry out rotations about the axes $\underset{\sim}{C}_1\underset{\sim}{C}_2'$, $\underset{\sim}{C}_1'\underset{\sim}{C}_2$, $\underset{\sim}{C}_1\underset{\sim}{C}_2$ and $\underset{\sim}{C}_1'\underset{\sim}{C}_2'$. These three stages of structural reorganization can be described as "bending", "folding" and "twisting" respectively [refs. 117, 118].

Figure 26 shows projections of clusters generated using a three dimensional hierarchical ballistic cluster-cluster aggregation model after zero, one, two and three stages of restructuring (IR = 0, 1, 2 and 3). Each cluster contains 4096 particles and the clusters are displayed on the same length scale. Measurements of the dependence of $\ln(R_g)$ on $\ln(s)$ for a large number of clusters indicate that the dependence of $R_g$ on s

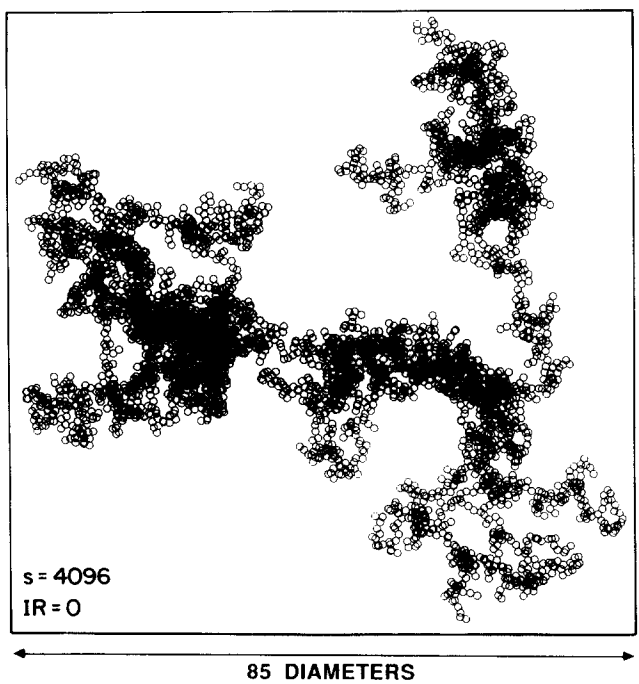


Fig. 26a.

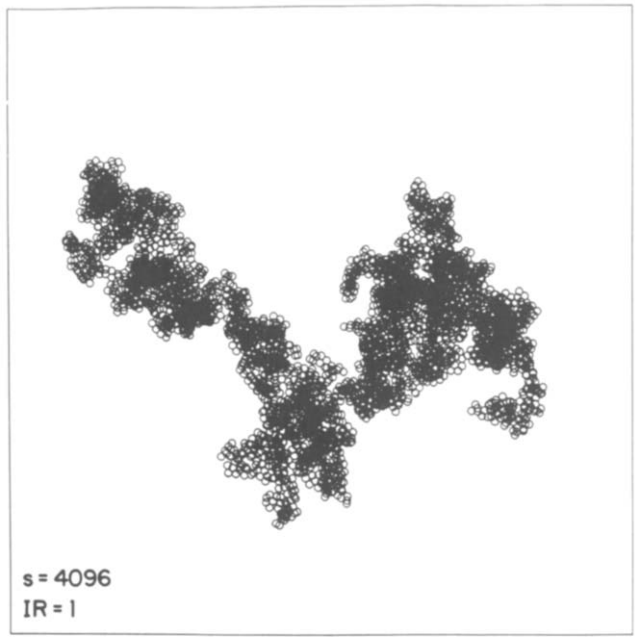


Fig. 26b.

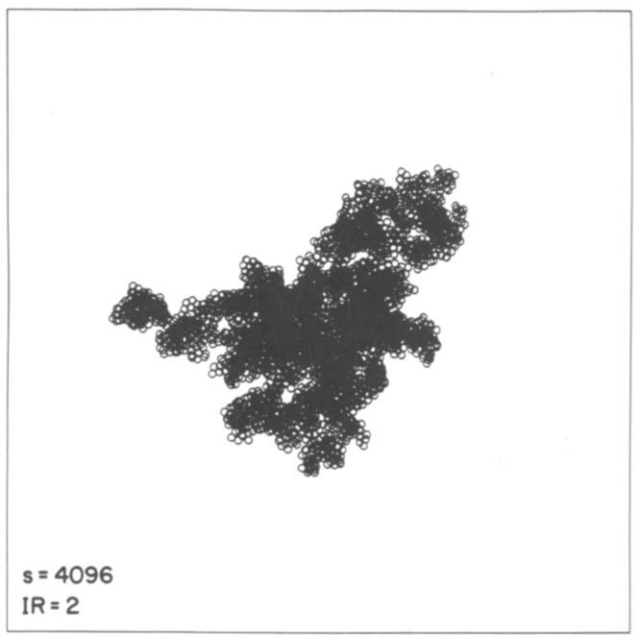


Fig. 26c.

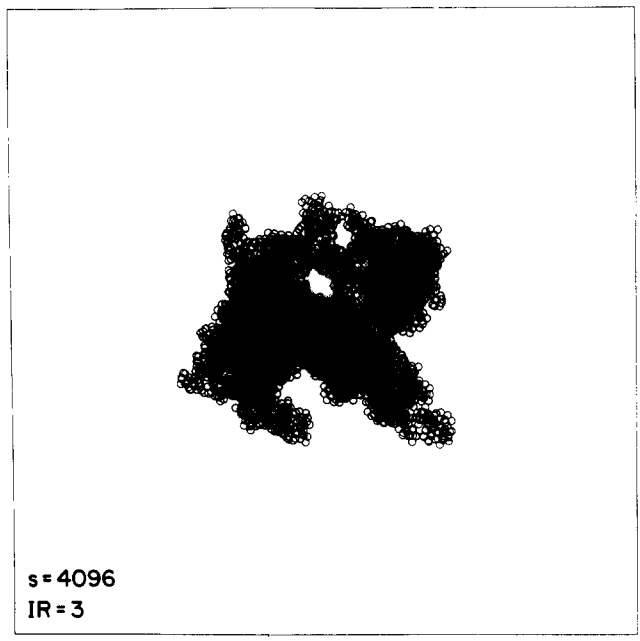


Fig. 26d.

Fig. 26. Clusters generated by a three-dimensional hierarchical model for ballistic cluster-cluster aggregation. The cluster shown in Figure 25a was obtained without restructuring. The clusters shown in Figures 25b, 25c and 25d were generated by simulations which included one stage (IR=1, bending), two stage (IR=2, bending + folding) and three stage (IR=3, bending + folding + twisting) of structural readjustments respectively. All four clusters contain 4096 particles and are shown on the same scale.

can be described by Equation (6) indicating that the clusters have a fractal geometry. It is evident from Figure 26 that there is a substantial change in the fractal dimensionality after one stage of restructuring followed by much smaller changes on going from IR = 1 to IR = 2 and from IR = 2 to IR = 3. From simulations in which a large number (200-1000) of 4096 particle clusters were generated, fractal dimensionalities (D) of 1.89, 2.08, 2.13 and 2.13 were obtained for IR = 0, 1, 2 and 3 respectively [ref. 117]. In all cases, the statistical uncertainty is much smaller than 0.01.

Similar simulations have been carried out using the polydisperse diffusion-limited [ref. 118], ballistic and reaction-limited cluster-cluster aggregation models described

above. The results of these simulations are given in Table I. After only one stage of restructuring the fractal dimensionality of three dimensional diffusion-limited aggregates increases from 1.80 to 2.09. This is indistinguishable from the fractal dimensionality obtained from reaction-limited aggregation simulations and illustrates the fact that measurement of the fractal dimensionality alone does not provide a unique determination of the aggregation mechanism. In this case, the two aggregation processes could easily be distinguished by measurements of the aggregation kinetics and/or cluster size distribution.

TABLE I

Fractal dimensionalities obtained from three-dimensional cluster-cluster aggregation models with smallest angle restructuring. The statistical uncertainties are smaller than 0.01 in all cases but systematic uncertainties may be larger than this.

| Model | Number of Restructuring Stages | | | |
|---|---|---|---|---|
| | IR=0 | IR=1 | IR=2 | IR=3 |
| Hierarchical Ballistic | 1.89 | 2.08 | 2.13 | 2.13 |
| Hierarchical Ballistic with Zero Impact Parameter | 2.04 | - | - | 2.21 |
| Polydisperse Diffusion-Limited | 1.80 | 2.09 | 2.17 | 2.18 |
| Polydisperse Ballistic | 1.95 | 2.13 | 2.18 | 2.19 |
| Polydisperse Reaction-Limited | 2.09 | 2.18 | 2.24 | 2.25 |

B. Reversible Aggregation

Although most fractal aggregates seem to be the result of essentially irreversible non-equilibrium processes, fractal structures can also result from reversible or partly reversible processes.

Meakin [ref. 120] investigated a lattice model for partially reversible diffusion-limited cluster-cluster aggregation. Here bonds which were not part of a loop of bonds or sites could be randomly broken. Both two and three dimensional simulations were carried out for a variety of bond breaking rate constants. These models result in the formation of structures which have a slightly higher effective fractal dimensionality than those generated by diffusion-limited cluster-cluster aggregation without bond breaking. The effect was found to be the largest for small bond breaking rate constants. For example, in two dimensional square lattice model simulations a fractal dimensionality of $1.52 \pm 0.03$ was obtained for the smallest bond breaking rate constant used. In general, large bond breaking

rate constants lead to many small loops and structures which are more compact on short length scales. Small bond breaking rate constants lead to fewer but larger loops. In all cases, the increase in the effective fractal dimensionality was found to be quite small and there may be no change in the asymptotic (large size limit) fractal dimensionality.

Botet and Jullien [ref. 122] investigated a model in which single bonded particles may escape from a cluster and undergo a random walk until they again reach the cluster. Starting with a variety of loopless structures they showed that the system evolves towards a steady state with a fractal dimensionality of $1.54\pm0.08$ irrespective of the starting configuration. This fractal dimensionality is numerically very close to that of two dimensional lattice animals [refs. 157,158]. However, Botet and Jullien found that the cluster statistics generated by this model are much different from that associated with lattice animals. To maintain a loopless structure in this model growth occurs when the randomly walking particle attempts to move from an unoccupied site onto a site occupied by the cluster. In this event the particle is joined only to that site which it attempted to occupy (even if there is more than one occupied nearest neighbor).

Kolb [ref. 121] developed a similar diffusion-limited cluster-cluster aggregation with random bond breaking. In this time dependent model a constant bond breaking rate is associated with each of the bonds. The system evolves towards a steady state in which the clusters have a fractal dimensionality of $1.57\pm0.06$ for d=2 and $2.03\pm0.05$ for d=3. Again, the fractal dimensionalities are equal or very close to those associated with two dimensional and three dimensional lattice animals respectively, but the cluster statistics depend on the model details.

Schaefer and Keefer [ref. 159] have used small angle x-ray scattering to investigate the fractal geometry of silica condensation polymers formed during the hydrolysis of silicon tetraethoxide ($Si(OC_2H_5)_4$). Fractal dimensionalities of $2.0\pm0.1$ were found for a variety of reaction conditions and extents of reaction. The results of these experiments were interpreted [ref. 159] in terms of lattice animals. Although the polymerization reaction seems to be irreversible under the conditions used, this or other similar systems may provide a

realization of Kolb's model.

C. Two Component Systems

A very wide variety of aggregation processes involve two or more distinct components. Although most of the recent simulation work has been directed towards single component systems and experiments on fractal aggregates have been concerned with systems which can be well approximated by single component models, there is a growing interest in multicomponent systems.

Meakin and Djordjevic [ref. 160] have developed both two dimensional and three dimensional lattice models for diffusion-limited cluster-cluster aggregation in two component (A-B) systems. In these models it is assumed that only sites representing unlike species can become irreversibly joined to each other. At the start of a simulation a fraction f of the sites is selected randomly to represent A particles and a fraction (1-f) is used to represent B particles. Clusters of indefinitely large sizes can be formed for only a limited range of compositions $0<f_1<f<f_2<1$. For compositions within this range the large clusters have the same fractal dimensionality as those generated by single component diffusion-limited aggregation

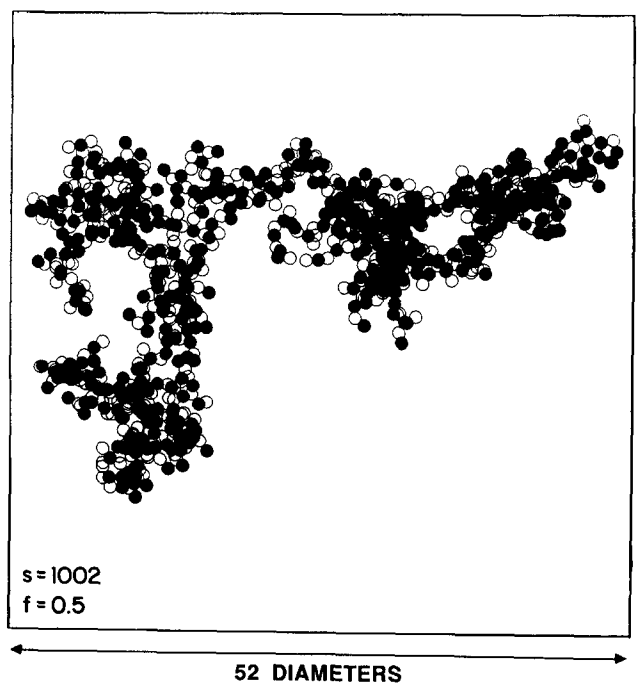


Fig. 27a.

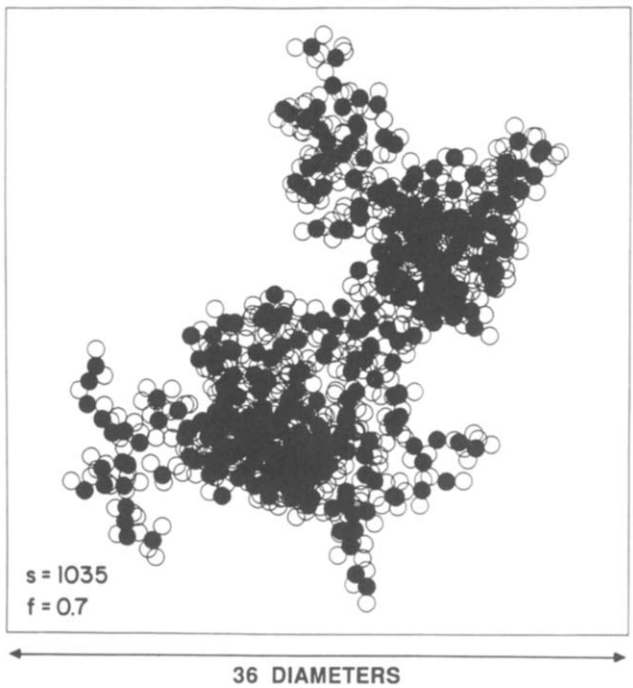


Fig. 27b.

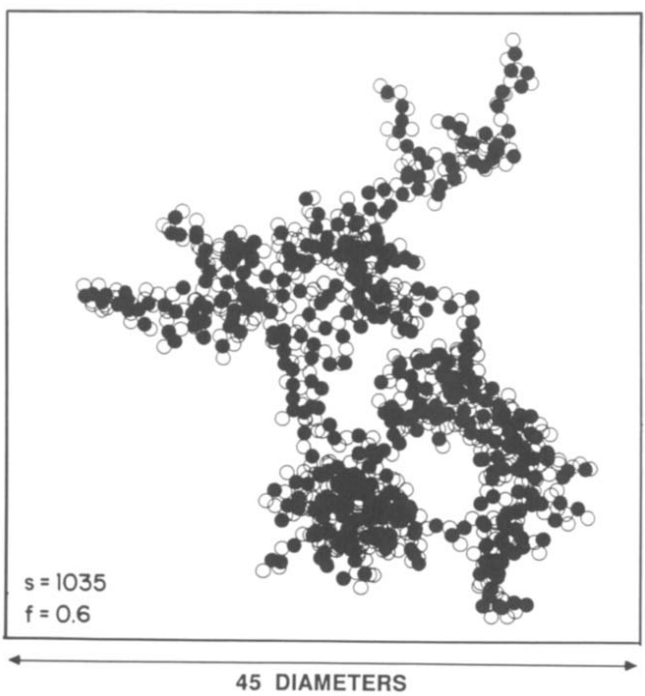


Fig. 27c.

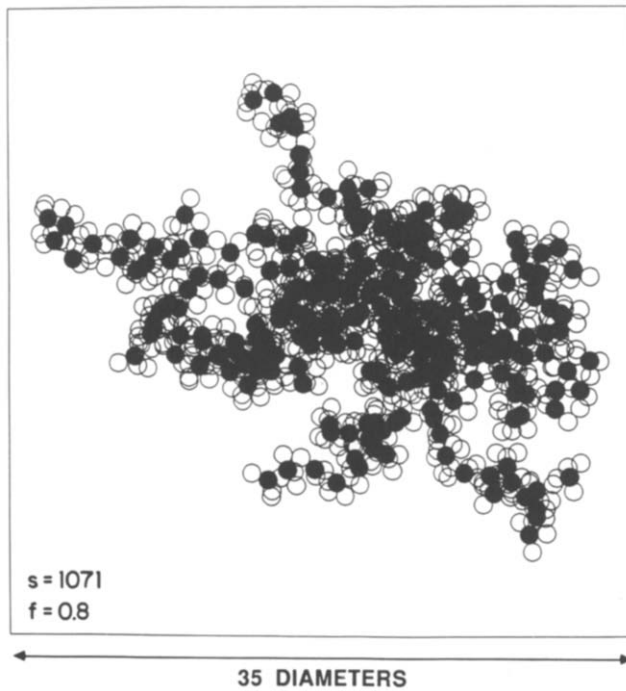


Fig. 27d.

Fig. 27. Clusters obtained from a three dimensional two species (A,B) model for reaction-limited cluster-cluster aggregation. In this model bonding is allowed only between particles of different kinds. In Figures 27a, 27b, 27c and 27d the fraction of A particles (indicated by open circles) is 0.5, 0.6, 0.7 and 0.8 respectively. In Figure 27d it can be seen that the cluster is almost completely coated by A particles.

models. However, as $f \to f_1$ or $f \to f_2$ the effective sticking probabilities of large clusters become quite small and the effective fractal dimensionality approaches that found for reaction-limited aggregation.

Outside of the range $f_1 < f < f_2$ the clusters grow to only a limited size and only certain nonconsecutive cluster sizes (s) are found. The specific structures formed depend on the functionalities of the A and B components.

Simulations have also been carried out using both lattice and off-lattice models for reaction-limited aggregation in two component systems (with A-B bonding only) [ref. 161]. Figure 26 shows some clusters generated using small scale off-lattice three dimensional simulations. These simulations were started with 10,000 particles of which a fraction f were of type A and a

fraction (1-f) of type B. The simulations were stopped whenever the largest cluster exceeded a size of 1000 particles and these clusters are shown in Figure 26 for four different values of f (0.5, 0.6, 0.7 and 0.8). As for the two component diffusion-limited aggregation models (lattice models) described above, large clusters are formed only for compositions in the range $f_1 < f < f_2$ ($f_2 = 1-f_2$). The compositions used to obtain Figures 26a-26d are within this range.

Figure 27 shows the cluster size distribution ($N_s(t)$) obtained at the stage where the total number of clusters had been reduced from $N_o$ = 200,000 to $N_o/8$ for f = 0.8. At this stage a large number of single particles remain (they are all A particles) but no doublets or triplets remain. Clusters containing 2 or 3 particles would contain at least one B particle

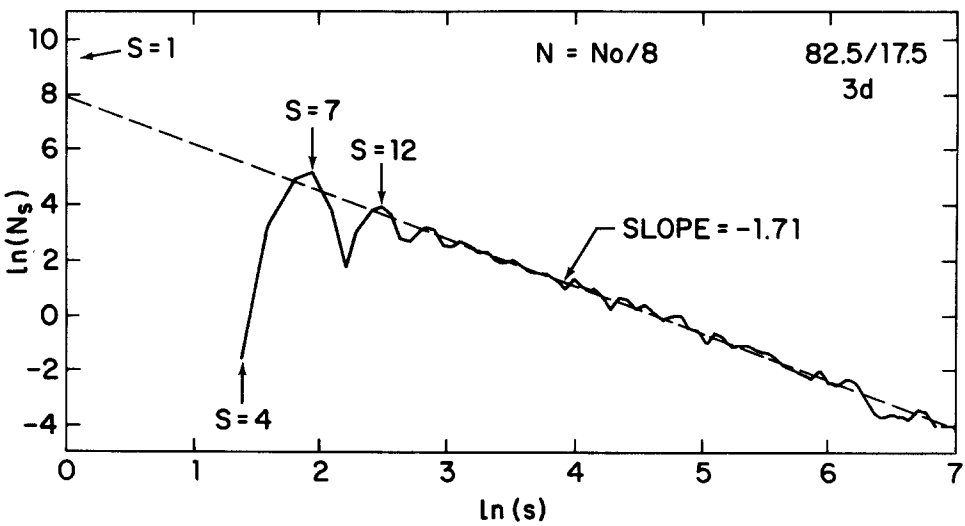


Fig. 28. The cluster size distribution ($N_s(t)$) obtained from a three dimensional off-lattice model for reaction-limited aggregation with two kinds of particles (A and B). The simulations were carried out with 82.5% A and 17.5% B particles, allowing only particles of different kinds to be joined. The cluster size distribution was obtained from five simulations. Each simulation was carried out using a total of 200,000 particles (160,000 A and 40,000 B). The cluster size distributions were determined at the stage where 25,000 clusters remained.

in a relatively exposed position. Such clusters are quite reactive to A particles and would be rapidly depleted. A maximum

is found at a cluster size (s) of seven particles. These are probably $A_6B$ clusters which can be formed relatively easily from $A_5B$ clusters by addition of an A particle. The $A_6B$ clusters are protected by a coating of A particles and are relatively unreactive in an A rich environment. A second maximum is found at s = 12. These 12 particle clusters must contain two B particles in which both B particles are quite well "protected" by A particles. Similar (but more pronounced) effects have also been found in the two species lattice models [ref. 160].

Jullien et al. [ref. 162] have recently developed a two dimensional reaction-limited aggregation model for the aggregation of particles by polymer bridging. In this model the particles are assumed to have a maximum functionality (f). The other parameters in the model are the number of polymers, the number of balls, the length of the polymer chains and the size of the box used in the simulation. If the number of polymers is large enough, all of the particles in a cluster may become saturated and the final state of the system may contain more than one aggregate. In this respect this model is similar to the two component model described above. In this model all of the polymer chains are constructed before they become attached to the particles. Preliminary results obtained from this model indicate that for at least some model parameters the fractal dimensionality may be larger than the value of 1.55 associated with two dimensional reaction-limited cluster-cluster aggregation.

D. Other Effects

Throughout this review I have tried to emphasize the fact that the formation of almost all aggregates involves the interaction between a variety of processes many of which can change the fractal dimensionality. One area of research which is becoming more active is the development of computer models to explore these processes and their implications for aggregate structure. In some cases fractal dimensionalities have been measured which do not agree with those associated with any of the simple models described above. In other cases the apparent agreement may be fortuitous since there is no reason to believe that aggregation is occurring under conditions which can be well represented by a simple model.

A good example is provided by the work of Hurd and Schaefer [ref. 136] on the aggregation of silica particles confined to an

air/water interface (Figure 28). The fractal dimensionality measured for the aggregates formed in this system was $1.20 \pm 0.15$ which is smaller than that which is characteristic of any of the simple two dimensional models discussed above. Hurd and Schaefer suggested that anisotropic repulsive interactions might be responsible for the low fractal dimensionality.

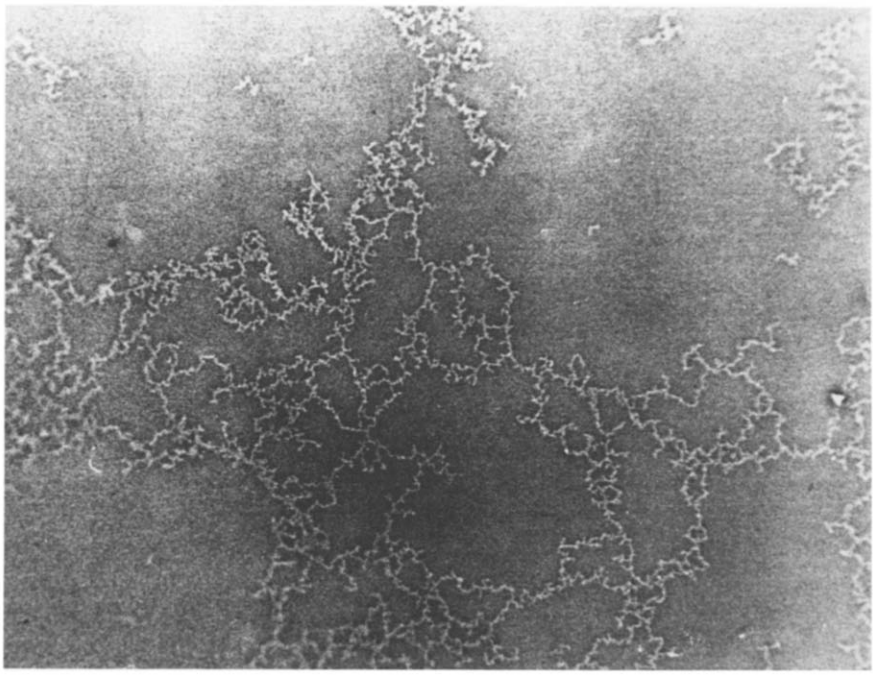

Fig. 29. A silica particle aggregate formed on an air/water interface. This picture was provided by A. J. Hurd.

Jullien [refs. 137 and 138] has proposed a simple model which seems to be consistent with the experimental results obtained by Hurd and Schaefer. In this hierarchical model a random direction is selected and pairs of clusters are brought together so that the particle in cluster 1 with the smallest projection in the selected direction is formed with the particle in cluster 2 with the largest projection in the same direction. This model generates aggregates with fractal dimensions of $1.26 \pm 0.06$ for $d = 2$, $1.42 \pm 0.05$ for $d = 3$ and $1.56 \pm 0.06$ for $d = 4$. Jullien suggested that this model may describe the experiments of Hurd and Schaefer because polarization of the clusters would cause

them to develop opposite charges at their nearest tips.

Mors, Botet and Jullien [ref. 139] have developed a three dimensional (hierarchical) cluster-cluster aggregation model in which dipolar interactions between the particles are included. In the large interaction limit fractal dimensionalities of about 1.35 were found for aggregations with and without relaxation of the directions of the dipole moments associated with the individual particles. Axelos et al. [ref. 163] have investigated the aggregation of colloidal aluminum hydroxide formed by the partial hydrolysis of aluminum chloride by sodium hydroxide. For $Al(OH)_{2.5}$ clusters, a fractal dimensionality of about 1.45 was found. They suggest that this result might be understood in terms of the attractive interaction model of Jullien [refs. 137 and 138].

Kim et al. [refs. 164 and 165] studied the aggregation of iron and cobalt particles and found fractal dimensionalities of about 1.34 and 1.72 respectively. The simulations of Mors et al. [ref. 134] indicate that D varies continuously with the particle magnetic moments from $D \simeq 1.35$ for large moments to $D \simeq 1.78$ for small moments. They suggested that the experimental results of Kim et al. may be consistent with their model and the idea that iron particles carry a large magnetic moment while the magnetic moment associated with the cobalt particles is small.

## X. CONCLUSIONS

In this review I have attempted to illustrate some of the recent advances which have been made towards developing a comprehensive understanding of the structure, formation and properties of fractal aggregates. The major emphasis has been on the contributions of computer simulations. There are several reasons for this. A large fraction of the work on fractal aggregates during recent years has been concerned with simulation results. I am more familiar with computer simulations than experimental work or theory and the computer models provide a convenient framework for discussing both experimental and theoretical work. A considerable number of experimental studies of aggregation processes leading to fractal structures have also been published during the past 5-10 years (most of them within the past 4 years). A few selected examples have been described and discussed above. However, in many cases the evidence for fractal geometry is weak and the systems are too complex to

obtain an unambiguous picture for the aggregation mechanism. In many cases it seems likely that the idealized models presented above are much too crude to provide an adequate representation of the physical and chemical processes occurring during aggregation. Nevertheless, some important experimental processes do seem to occur under conditions which closely approximate those explicitly or implicitly assumed in the computer models. It is these processes which have been emphasized.

## XI. ACKNOWLEDGMENTS

This review would not have been possible without the contributions of a large number of colleagues. In particular, I would like to thank those who have collaborated with me on the topics discussed in this review. These collaborations have enhanced my understanding of, interest in, and enjoyment of these areas. Work on ballistic deposition has been carried out with R. C. Ball, R. Jullien, L. M. Sander and P. Ramanlal. M. H. Ernst, F. Family, E. D. McGrady, T. Vicsek and R. M. Ziff have collaborated with me on and taught me most of what I know about aggregation kinetics. Work on ballistic cluster-cluster aggregation was carried out with B. Donn and the work on reaction-limited aggregation with F. Family. Almost all of the work on restructuring was carried out with R. Jullien and the work on two-component systems with Z. Djordjevic and S. Miyazima. I would also like to thank A. J. Hurd, J. E. Martin, G. W. Mulholland, A. J. Skjeltorp and D. A. Weitz for providing figures.

## XII. APPENDIX

Much of the recent work on fractals has been carried out by Physicists (primarily those with a background in statistical physics). As a result, the terminology used in this review is somewhat different than that which is used in the mainstream of colloid science. In particular, the term "fractal aggregates" is applied to a very broad range of random structures (almost irrespective of their properties or origin). For example, random structures formed by processes such as dielectric breakdown, electrodeposition and random dendritic growth are often called "aggregates". Most of this review has been concerned with the structure and properties of flocs (a term which is almost never used in the physics literature).

Since this is a young area there is no standard system of nomenclature. Following Mandelbrot [refs. 2-4], fractal dimensionalities have been indicated by "D" and Euclidean dimensionalities by "d" throughout this review (with appropriate subscripts or superscripts when there is a need to be more specific). As a result, I have resorted to using the symbol $\mathcal{D}$ to indicate diffusion coefficients. In most cases symbols are defined as they are used in the text. However, the list of symbols given below may be of some help in those cases where they are not defined in the text or are used infrequently throughout the text.

A. List of Symbols

| | |
|---|---|
| $A_c$ | Screening coefficient in screened growth model |
| $\mathring{A}$ | Angstrom ($10^{-10}$ meters) |
| B(t) | Brownian Process |
| $C_N$ | Number of bonding configurations between pairs of clusters each containing N sites or particles |
| C(r) | Two point density-density correlation function |
| d | Euclidean dimensionality |
| D | Fractal dimensionality |
| $D_G$ | Global ($\ell \to \infty$) fractal dimensionality |
| $D_L$ | Local ($\ell \to 0$) fractal dimensionality |
| $D_{min}$ | Dimensionality characterizing scaling relationship between the minimum path length between two points on a fractal and their separation measured in the embedding space or lattice |
| $d_o$ | Particle diameter |
| $D_s$ | Spectral or fracton dimensionality |
| $D_w$ | Fractal dimensionality of path, walk or trajectory |
| $D_\alpha$ | Fractal dimensionality obtained from density-density correlation function |
| $D_\beta$ | Fractal dimensionality obtained from dependence of radius of gyration on mass |
| $D_\gamma$ | Fractal dimensionality obtained from mass within a distance $\ell$ measured from an occupied point |
| $D_{\mathcal{D}}$ | Fractal dimensionality obtained from dependence of density on mass |
| Fo(n) | Probability that a random walk will return to its origin after n steps |
| f(x) | Scaling function |

| | |
|---|---|
| $h$ | Height |
| $k$ | Wave vector |
| $\underset{\approx}{K}$ | Force constant matrix |
| $K(i,j)$ | Element of Smoluchowski equation reaction kernel for addition of clusters of size i and j |
| $\ell$ | Length |
| $L$ | Strip width for simulation with periodic boundary conditions |
| $M$ | Mass |
| $N$ | Number of particles or occupied lattice sites |
| $N(r)$ | Number of boxes of size r required to cover a fractal |
| $N_s(t)$ | Number of clusters of size s at time t |
| $N(\omega)$ | Vibrational density of states |
| $P$ | Probability |
| $Q(i,j)$ | Upper limit to collision cross-section in ballistic cluster-cluster aggregation |
| $r$ | Distance |
| $r_o$ | Radius of particles |
| $R_g$ | Radius of gyration |
| $R_h$ | Hydrodynamic radius |
| $R_o$ | Radius of aggregate |
| $R_z$ | z average cluster radius |
| $s$ | Number of particles or sites in an aggregate or walk |
| $S$ | Mean cluster size (weight average) |
| $t$ | Time |
| $t_g$ | Gelation time |
| $\underset{\approx}{W}$ | Transition probability matrix in master equation |
| $X$ | Random number uniformly distributed over the range $0 \leqslant X \leqslant 1$ |
| $z$ | Exponent describing algebraic growth of mean cluster size (S(t)) |
| $\alpha$ | Exponent characterizing power law density-density correlation function. This quantity is also known as the codimension |
| $\alpha'$ | Exponent describing dependence of surface thickness ($\xi$) on strip width (L) |
| $\beta$ | Exponent relating radius of gyration ($R_g$) to cluster size (S, N or M) |
| $\beta'$ | Exponent describing dependence of surface thickness ($\xi$) on height |
| $\gamma$ | Exponent relating mass contained within a distance $\ell$ to $\ell$ |

| | |
|---|---|
| $\gamma'$ | Exponent in scaling relationship between diffusion coefficient and mass |
| $\delta$ | Displacement |
| $\varepsilon$ | Exponent in the screening function for the screened growth and Rikvold models |
| $\xi$ | Surface thickness (variance in surface height) |
| $\eta$ | Correction term exponent characterizing dependence of the projected area ($\sigma$) on the cluster size (s) |
| $\Theta$ | Scattering angle |
| $\Theta'$ | Exponent characterizing divergence of the mean cluster size as time approaches the gelation time $t_g$ |
| $\lambda$ | Cut-off length for screening function in Rikvold's model |
| $\lambda'$ | Homogeneity index for reaction kernel |
| $\mathcal{K}$ | Exponent associated with the dependence of density on aggregate mass |
| $\mu$ | Scaling exponent for reaction kernel K(i,j) |
| $\nu$ | Scaling exponent or reaction kernel K(i,j) |
| $\nu'$ | Exponent characterizing dependence of projected area ($\sigma$) on the cluster size (s) |
| $\rho$ | Density |
| $\sigma$ | Area of projection onto a plane |
| $\sigma'$ | Sticking probability |
| $\tau$ | Exponent characterizing power law cluster size distribution |
| $\omega$ | Frequency |
| $\omega'$ | Exponent characterizing the dependence of the number of bonding configurations ($C_N$) on the cluster size (N or s) in reaction-limited cluster-cluster aggregation |
| $\mathcal{D}$ | Diffusion coefficient |
| $< >$ | Ensemble average |

## XIII. REFERENCES


1 D. A. Weitz and M. Oliveria, Phys. Rev. Lett. 52, 1433 (1984).
2 B. B. Mandelbrot, "The Fractal Geometry of Nature", W. H. Freeman and Company, New York (1982).
3 B. B. Mandelbrot, "Les Objets Fractals: Forme et Dimension", Flammarion, Paris (1975).
4 B. B. Mandelbrot, "Fractals: Form, Chance and Dimension" W. H. Freeman, San Francisco (1977).
5 H. O. Peitgen and P. H. Richter, "The Beauty of Fractals: Images of Complex Dynamical Systems", Springer-Verlag, Berlin (1986).
6 K. J. Falconer, "The Geometry of Fractal Sets", Cambridge University Press, Cambridge (1985).
7 J. Feder, "Fractals", Plenum Press (1988).
8 K. Honda, Fractals in Physics, Osakura Shoten (1987).

9 R. Jullien and R. Botet, Aggregation and Fractal Aggregates, World Scientific, Singapore (1986).
10 F. Family and D. P. Landau, eds., Kinetics of Aggregation and Gelation, North Holland, Amsterdam (1984).
11 H. E. Stanley and N. Ostrowsky, eds., "On Growth and Form: Fractal and Non-Fractal Patterns in Physics", NATO ASI, Series E100, Martinus Nijhoff, Dordrecht (1986).
12 L. Pietronero and E. Tosatti, eds., "Fractals in Physics", Proceedings of the Sixth Trieste International Symposium on Fractals in Physics, ICTP Trieste, Italy, North Holland, Amsterdam (1986).
13 M. Shlesinger, Proceedings of a Conference on Fractals in the Physical Sciences, NBS, Gaithersburg, MD (1984) (J. Stat. Phys. Vol. 36, No 8/6).
14 R. Pynn and A. T. Skjeltorp, "Scaling Phenomena in Disordered Systems" NATO ASI Series B133, Plenum Press, New York (1986).
15 T. Riste and R. Pynn, "Time Dependent Effects in Disordered Materials" NATO ASI, Series B, Plenum Press, New York (1987).
16 H. J. Herrmann, Physics Reports 136, No. 3, 153 (1986).
17 R. Jullien, R. Botet and M. Kolb, La Recherche 171, 1334 (1986).
18 R. Jullien, Ann. Telecommun. 41, 343 (1986).
19 L. M. Sander, Nature 322, 789 (1986).
20 L. M. Sander, Scientific American 256 (1), 94 (1987).
21 M. LaBrecque, Mosaic 17, No. 4, 34 (1986/7).
22 M. LaBrecque, Mosaic 18, No. 2, 22 (1987).
23 R. Orbach, Science 231, 814 (1986).
24 S. H. Liu, Solid State Physics, H. Ehrenreich, F. Seitz and D. Turnbull, eds., Academic Press, New York (1986).
25 T. A. Witten and M. E. Cates, Science 232, 1607 (1986).
26 P. Meakin, Phase Transition and Critical Phenomena, C. Domb and J. L. Lebowitz, eds., Vol. 12, Academic Press, New York (1988).
27 T. A. Witten and L. M. Sander, Phys. Rev. Lett. 47, 1400 (1981).
28 T. Vicsek, J. Phys. A16, L647 (1983).
29 E. E. Fournier, D'Albe, Two New Worlds. I. The Infra World. II. The Supra World, Longmans Green, London (1907).
30 Y. Kantor and T. A. Witten, J. Physique Lett. 45, L675 (1984).
31 H. M. Lindsay, M. Y. Lin, D. A. Weitz, P. Sheng, Z. Chen, R. Klein and P. Meakin, Faraday Discuss. Chem. Soc. No. 83, 153 (1987).
32 H. E. Stanley, J. Phys. A10, L211 (1977).
33 B. B. Mandelbrot in "Fractals in Physics", Proceedings on Sixth International Symposium on Fractals in Physics - ICTP. L. Pietronero and E. Tosatti, eds., North Holland, Amsterdam (1986).
34 F. Family and T. Vicsek, J. Phys. A18, L75 (1985).
35 P. Meakin, CRC Critical Reviews in Solid State and Material Science 13, 143 (1987).
36 B. B. Mandelbrot, D. E. Passoja and A. J. Paullay, Nature 308, 721 (1984).
37 M. J. Vold, J. Colloid Sci. 14, 168 (1959).
38 M. Eden, Proceedings of the Fourth Berkeley Symposium on Math., Statistics and Probability, F. Neyman, ed. (1961) (Univ. of Calif. Press, Berkeley).
39 B. B. Mandelbrot, Physica Scripta 32, 257 (1985).
40 R. F. Voss in "Scaling Phenomena in Disordered Systems" NATO ASI, Series B133, R. Pynn and A. Skjeltorp, eds., Plenum Press, New York (1986).

41 S. Alexander in "Transport and Relaxation in Random Materials" J. Klafter, R. J. Rubin and M. S. Shlesinger, eds., World Scientific Publications, Singapore (1986).
42 K. M. Middlemiss, S. G. Whittington and D. S. Gaunt, J. Phys. A13, 1835 (1980).
43 R. Pike and H. E. Stanley, J. Phys. A14, L169 (1981).
44 Y. Gefen, A. Aharony and S. Alexander, Phys. Rev. Lett. 50, 77 (1983).
45 S. Havlin and D. Ben-Avraham, Adv. in Physics, 36, 695 (1987).
46 S. Alexander and R. Orbach, J. Physique Lett. 43, L625 (1982).
47 R. Rammal and G. Toulouse, J. Physique Lett. 44, L13 (1983).
48 C. Kittel, Introduction to Solid State Physics (Sixth Edition) John Wiley and Sons, Inc., New York (1986).
49 S. Alexander, J. Bernasconi, W. R. Schneider and R. Orbach, Rev. Mod. Phys. 53, 175 (1981).
50 R. Orbach, ref. 14, p. 335 (1986).
51 A. Aharony, O. Entin-Wohlman and R. Orbach in "Time Dependent Effects in Disordered Materials", NATO ASI, Geilo, Norway. T. Riste and R. Pynn, eds. (1987).
52 P. Dimon, S. K. Sinha, D. A. Weitz, C. R. Safinya, G. S. Smith, W. A. Varady and H. M. Lindsay, Phys. Rev. Lett. 57, 595 (1986).
53 J. E. Martin and A. J. Hurd, J. Appl. Cryst. 20, 61 (1987).
54 M. V. Berry and I. C. Percival, Optica Acta 33, 577 (1986).
55 Z.-Y. Chen, P. Weakliem, W. Gelbart and P. Meakin, Phys. Rev. Lett. 58, 1966 (1987).
56 G. Seeley, T. Keyes, and T. Ohtsuki, Phys. Rev. Lett. 60, 290 (1988).
57 H. M. Lindsay, R. Klein, D. A. Weitz, M. Y. Lin and P. Meakin, in ref. 15.
58 Y. Gefen, B. B. Mandelbrot and A. Aharony, Phys. Rev. Lett. 45, 855 (1980).
59 M. J. Vold, J. Colloid Sci. 18, 684 (1963).
60 D. N. Sutherland, J. Colloid Interface Sci. 22, 300 (1966).
61 P. Meakin, J. Colloid Interface Sci., 105, 240 (1985).
62 D. Bensimon, B. Shraiman and S. Liang, Phys. Lett. 102A, 238 (1984).
63 R. C. Ball and T. A. Witten, Phys. Rev. A29, 2966 (1984).
64 R. C. Ball and T. A. Witten, J. Stat. Phys. 36, 873 (1984).
65 M. J. Vold, J. Phys. Chem. 63, 1608 (1959).
66 R. Jullien and P. Meakin, Europhys. Lett. 4, 1385 (1987).
67 M. Kardar, G. Parisi and Y.-C. Zhang, Phys. Rev. Lett. 56, 889 (1986).
68 P. Meakin, P. Ramanlal, L. M. Sander and R. C. Ball, Phys. Rev. A34, 5091 (1986).
69 P. Meakin and R. Jullien, J. de Physique 48, 1651 (1987).
70 P. Meakin, J. Phys. A20, L1113 (1987).
71 D. N. Sutherland, J. Colloid Interface Sci. 25, 373 (1967).
72 D. N. Sutherland, Nature 226, 1241 (1970).
73 D. N. Sutherland and I. Goodarz-Nia, Chem. Eng. Sci., 26, 2071 (1971).
74 M. Von Smoluchowski, Z. Phys. 17, 585 (1916).
75 M. Von Smoluchowski, Z. Phys. Chem. 92, 129 (1917).
76 P. Meakin and B. Donn, preprint.
77 R. Jullien and P. Meakin, preprint.
78 J. M. Beeckmans, Ann. Occup. Hyg. 7, 299 (1964).
79 A. I. Medalia and F. A. Beckman, J. Colloid Interface Sci. 36, 173 (1971) and references therein.

80 A. I. Medalia, Surface and Colloid Sci. 4, 1 (1971) and references therein.
81 A. I. Medalia in Testing and Characterization of Powders and Fine Particles, 67 and references therein, J. K. Beddow et al. eds., Heyden, Philadelphia (1980).
82 A. I. Medalia, J. Colloid Interface Sci. 24, 393 (1967).
83 F. A. Heckman and A. I. Medalia, Carbon 7, 567 (1969).
84 D. Richardson, Proc. Cambridge Philos. Soc. 74, 515 (1973).
85 R. Jullien and R. Botet, Phys. Rev. Lett. 54, 2055 (1985).
86 R. Jullien and R. Botet, J. Phys. A18, 2279 (1985).
87 P. Freche, D. Stauffer and H. E. Stanley, J. Phys. A18, L1163 (1985).
88 R. Hirsch and D. E. Wolf, J. Phys. A19, L251 (1986).
89 M. Plischke and Z. Racz, Phys. Rev. Lett. 53, 415 (1984).
90 M. Plischke and Z. Racz, Phys. Rev. A32, 3825 (1985).
91 J. G. Zabolitsky and D. Stauffer, Phys. Rev. A34, 1523 (1986).
92 D. Stauffer and J. G. Zabolitzky, Phys. Rev. Lett. 57, 1809 (1986).
93 D. E. Wolf and J. Kertesz, J. Phys. A20, L257 (1987).
94 D. E. Wolf and J. Kertesz, Europhys. Lett. 4, 651 (1987).
95 S. Tolman and P. Meakin, unpublished.
96 R. C. Ball, Physica 62 (1987). Invited lectures presented at the 16th International Conference on Thermodynamics and Statistical Physics, Boston University (1986) H. E. Stanley, ed.
97 P. Meakin, Disc. Faraday Soc. No. 83 (1987).
98 P. Meakin, Phys. Rev. A34, 710 (1986).
99 P. A. Rikvold, Phys. Rev. A26, 647 (1982).
100 P. Meakin, Phys. Rev. B28, 6718 (1983).
101 P. Meakin, F. Leyvraz and H. E. Stanley, Phys. Rev. A31, 1195 (1985).
102 L. M. Sander in "Kinetics of Aggregation and Gelation", F. Family and D. P. Landau, eds., North Holland, Amsterdam p. 13 (1984).
103 P. Meakin, preprint (1987).
104 J. Kertesz and T. Vicsek, J. Phys. A19, L257 (1986).
105 J. Nittmann and H. E. Stanley, Nature 321, 663 (1986).
106 J. D. Chen and D. Wilkinson, Phys. Rev. Lett. 55, 1892 (1985).
107 P. Meakin, preprint.
108 A. T. Skjeltorp, Phys. Rev. Lett. 58, 1444 (1987).
109 P. Meakin, Phys. Rev. B29, 3722 (1984).
110 P. Meakin, unpublished.
111 P. Meakin, Phys. Rev. Lett. 51, 1119 (1983).
112 M. Kolb, R. Botet and R. Jullien, Phys. Rev. Lett. 51, 1123 (1983).
113 L. X. Finegold, Biochem. Biophys. Acta 448, 393 (1976).
114 J. T. Donnell and L. X. Finegold, Biophys. J. 35, 783 (1981).
115 H. Sunada, A. Otsuka, Y. Yamada, Y. Kawashima, H. Takeonaka and J. T. Carstensen, Powder Technol. 38, 211 (1984).
116 P. Meakin and R. Jullien, J. Physique 46, 1543 (1985).
117 R. Jullien and P. Meakin, preprint.
118 P. Meakin and R. Jullien, preprint.
119 P. Meakin, J. Colloid Interface Sci. 112, 187 (1986).
120 P. Meakin, J. Chem. Phys. 83, 3645 (1985).
121 M. Kolb, J. Phys. A19, L263 (1986).
122 R. Botet and R. Jullien, Phys. Rev. Lett. 55, 1943 (1985).
123 P. Meakin and Z. R. Wasserman, Phys. Lett. 103A, 337 (1984).
124 R. M. Ziff, E. D. McGrady and P. Meakin, J. Chem. Phys.

125 T. Vicsek and F. Family, Phys. Rev. Lett. 53, 2281 (1984).
126 M. Kolb, Phys. Rev. Lett. 53, 1653 (1984).
127 R. Botet and R. Jullien, J. Phys. A17, 2517 (1984).
128 P. Meakin, T. Vicsek and F. Family, Phys. Rev. B31, 564 (1984).
129 D. A. Weitz, J. S. Huang, M. J. Lin and J. Sung, Phys. Rev. Lett. 53, 1657 (1984).
130 P. G. J. van Dongen and M. H. Ernst, Phys. Rev. Lett. 54, 1396 (1985).
131 F. Leyvraz in "On Growth and Form: Fractal and Non-fractal Patterns in Physics" NATO ASI Series E100, H. E. Stanley and N. Ostrowsky, eds., Martinus Nijhoff, Dordrecht (1986).
132 P. G. J. Van Dongen, Kinetic Theory of Coagulation, Thesis, Utrecht University, The Netherlands (1987).
133 S. R. Forrest and T. A. Witten, J. Phys. A12, L109 (1979).
134 D. Shonauer and U. Kreibig, Surface Science, 156, 100 (1985).
135 D. W. Schaefer, J. E. Martin, P. Wiltzius and D. S. Cannell, Phys. Rev. Lett. 52, 2371 (1984).
136 A. J. Hurd and D. W. Schaefer, Phys. Rev. Lett. 54, 1043 (1985).
137 R. Jullien, Phys. Rev. Lett. 55, 1697 (1985).
138 R. Jullien, J. Phys. A19, 2129 (1986).
139 P. M. Mors, R. Botet and R. Jullien, J. Phys. A20, L975 (1987).
140 J. Jeans "The Dynamical Theory of Gases", Dover, New York (1954).
141 R. J. Samson, G. W. Mulholland and J. W. Gentry, Langmuir 3, 272 (1987).
142 A. J. Hurd, D. W. Schaefer and J. E. Martin, Phys. Rev. A35, 2361 (1987).
143 M. Tence, J. P. Chevalier and R. Jullien, J. Physique 47, 1989 (1986).
144 R. C. Ball, D. A. Weitz, T. A. Witten and F. Leyvraz, Phys. Rev. Lett. 58, 274 (1987).
145 M. Kolb and R. Jullien, J. Physique Lett. 45, L977 (1984).
146 R. Jullien and M. Kolb, J. Phys. A17, L639 (1984).
147 W. D. Brown and R. C. Ball, J. Phys. A18, L517 (1985).
148 F. Leyvraz, preprint.
149 P. Meakin and F. Family, Phys. Rev. A36, 5498 (1987).
150 P. Meakin and F. Family
151 J. E. Martin, Phys. Rev. A36, 3415 (1987).
152 C. K. Von Schulthess, G. B. Benedek and R. W. de Blois, Macromolecules 13, 939 (1980).
153 D. A. Weitz, J. S. Huang, M. Y. Lin and J. Sung, Phys. Rev. Lett. 54, 1416 (1985).
154 J. G. Rarity, Faraday Disc. Chem. Soc. No. 83, 234 (1987).
155 D. W. Schaefer, J. E. Martin, P. Wiltzius and D. S. Cannell, Phys. Rev. Lett. 52, 2371 (1984).
156 C. Aubert and D. S. Cannell, Phys. Rev. Lett. 56, 738 (1986).
157 D. Stauffer, Introduction to Percolation Theory, Taylor and Francis, London (1985).
158 F. Harary, Graph Theory and Theoretical Physics, Academic, London (1967).
159 D. W. Schaefer and K. D. Keefer, Phys. Rev. Lett. 53, 1383 (1984).
160 P. Meakin and Z. D. Djordjevic, J. Phys. A19, 2137 (1986).
161 P. Meakin and S. Miyazima, preprint.
162 R. Jullien, R. Botet and P. M. Mors, Faraday Discuss, Chem. Soc., No. 83, 125 (1987).

163 M. A. V. Axelos, D. Tchoubar and R. Jullien, J. Physique, 47, 1843 (1986).
164 S. G. Kim and J. R. Brock, J. Applied Phys. 60, 509 (1986).
165 S. G. Kim and J. R. Brock, J. Colloid Interface Sci. 116, 431 (1987).